Article

Cell

Protein AMPylation by an Evolutionarily Conserved Pseudokinase

Graphical Abstract

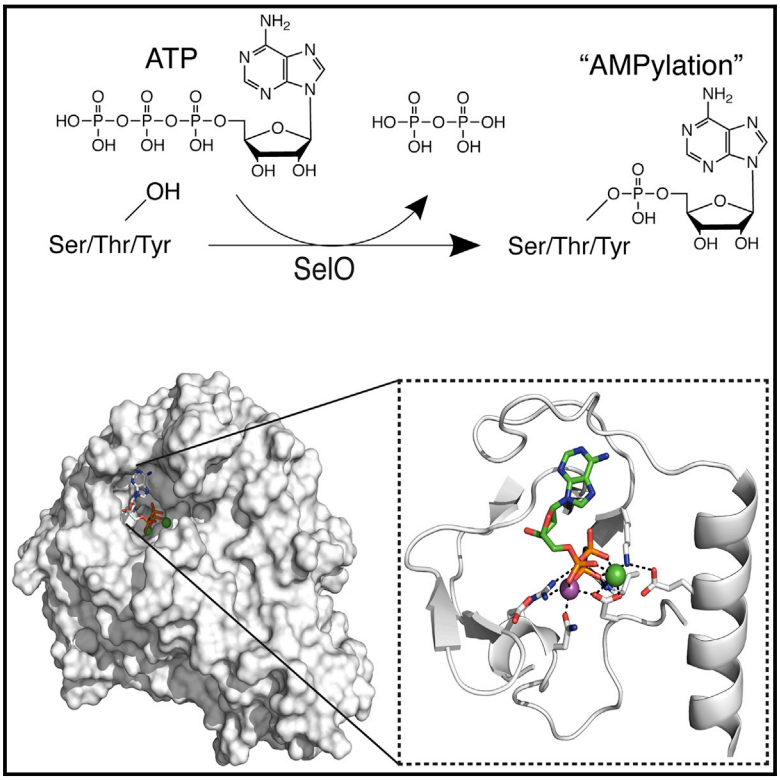

Highlights

- SelO adopts a protein kinase fold with ATP flipped in the active site
- SelO transfers AMP to Ser, Thr, and Tyr residues on protein substrates (AMPylation)
- SelO AMPylates proteins involved in redox homeostasis
- SelO protects cells from oxidative stress and regulates protein glutathionylation

Authors

Anju Sreelatha, Samantha S. Yee, Victor A. Lopez, ..., Krzysztof Pawłowski, Diana R. Tomchick, Vincent S. Tagliabracci

Correspondence

vincent.tagliabracci@utsouthwestern.edu

In Brief

The structure of SelO, a conserved pseudokinase, reveals ATP flipped in the substrate binding pocket, leading to the discovery that SelO is actually an AMPylating enzyme.

Sreelatha et al., 2018, Cell *175*, 809–821
October 18, 2018
https://doi.org/10.1016/j.cell.2018.08.046

CellPress

Article

Cell

Protein AMPylation by an Evolutionarily Conserved Pseudokinase

Anju Sreelatha,[1] Samantha S. Yee,[1,9] Victor A. Lopez,[1] Brenden C. Park,[1] Lisa N. Kinch,[5] Sylwia Pilch,[3] Kelly A. Servage,[1] Junmei Zhang,[1,10] Jenny Jiou,[2] Monika Karasiewicz-Urbańska,[4] Małgorzata Łobocka,[3,4] Nick V. Grishin,[2,5,6] Kim Orth,[1,5,6] Roza Kucharczyk,[3] Krzysztof Pawłowski,[4] Diana R. Tomchick,[2,6] and Vincent S. Tagliabracci[1,7,8,11,*]

[1]Department of Molecular Biology, University of Texas Southwestern Medical Center, Dallas, TX 75390, USA
[2]Department of Biophysics, University of Texas Southwestern Medical Center, Dallas, TX 75390, USA
[3]Institute of Biochemistry and Biophysics, Polish Academy of Sciences, Warsaw 02-106, Poland
[4]Faculty of Agriculture and Biology, Warsaw University of Life Sciences, Warsaw 02-776, Poland
[5]Howard Hughes Medical Institute, Dallas, TX 75390, USA
[6]Department of Biochemistry, University of Texas Southwestern Medical Center, Dallas, TX 75390, USA
[7]Harold C. Simmons Comprehensive Cancer Center, University of Texas Southwestern Medical Center, Dallas, Texas 75390, USA
[8]Hamon Center for Regenerative Science and Medicine, University of Texas Southwestern Medical Center, Dallas, Texas 75390, USA
[9]Present address: Department of Pharmacology, The University of Texas Health Science Center at San Antonio, San Antonio, Texas 78229-3900, United States
[10]Present address: Department of Pharmaceutical Sciences, School of Pharmacy, University of Pittsburgh, Pittsburgh, PA 15261, USA
[11]Lead Contact
*Correspondence: vincent.tagliabracci@utsouthwestern.edu
https://doi.org/10.1016/j.cell.2018.08.046

SUMMARY

Approximately 10% of human protein kinases are believed to be inactive and named pseudokinases because they lack residues required for catalysis. Here, we show that the highly conserved pseudokinase selenoprotein-O (SelO) transfers AMP from ATP to Ser, Thr, and Tyr residues on protein substrates (AMPylation), uncovering a previously unrecognized activity for a member of the protein kinase superfamily. The crystal structure of a SelO homolog reveals a protein kinase-like fold with ATP flipped in the active site, thus providing a structural basis for catalysis. SelO pseudokinases localize to the mitochondria and AMPylate proteins involved in redox homeostasis. Consequently, SelO activity is necessary for the proper cellular response to oxidative stress. Our results suggest that AMPylation may be a more widespread post-translational modification than previously appreciated and that pseudokinases should be analyzed for alternative transferase activities.

INTRODUCTION

Protein kinases are an important class of enzymes that transfer phosphate from ATP to protein substrates, a process known as phosphorylation (Fischer, 2013). Virtually every cellular activity is regulated by protein kinases, and abnormal phosphorylation has been linked to numerous diseases. More than 500 human protein kinases have been identified and assembled into an evolutionary tree known as the human kinome (Manning et al., 2002). However, research is largely biased toward kinases with well-established roles in disease; it has been estimated that the molecular functions of more than 50% of human kinases remain uncharacterized (Fedorov et al., 2010). Furthermore, several new kinase families have been identified that are so different they were not included on the human kinome tree. These include the Fam20 and Fam69 families of secretory pathway kinases (Dudkiewicz et al., 2013; Tagliabracci et al., 2012) and the selenocysteine (Sec)-containing protein selenoprotein-O (SelO) (Dudkiewicz et al., 2012).

About 10% of human protein kinases are predicted to be inactive and referred to as pseudokinases because they are missing residues located in highly conserved sequence motifs believed to be required for ATP binding and catalysis (Manning et al., 2002). Pseudokinases serve a multitude of non-catalytic roles, such as allosteric regulators or scaffolding functions (Eyers and Murphy, 2013; Kung and Jura, 2016; Taylor et al., 2013; Zeqiraj and van Aalten, 2010). For example, the Fam20A pseudokinase binds to and increases the stability and activity of the secretory pathway kinase Fam20C, thus acting as an allosteric regulator (Cui et al., 2015). Similarly, the HER3 pseudokinase, although reported to have low catalytic activity, serves mostly as an allosteric activator for other members of the EGFR family of receptor kinases (Jura et al., 2009; Shi et al., 2010). These studies have highlighted the importance of pseudokinases in human biology, and their diverse signaling functions make them attractive drug targets (Bailey et al., 2015; Byrne et al., 2017).

Pseudokinases were initially predicted to be inactive if they were missing one or more of the three critical residues known to participate in phosphotransfer in active kinases (Manning et al., 2002). These include (1) the VAIK motif in the β3-strand, where the Lys positions the α and β phosphates of ATP for catalysis (K72 using protein kinase A; PKA nomenclature); (2) the HRD motif located in the catalytic loop, where the Asp acts as the catalytic base (PKA; D166); and (3) the DFG motif; where the

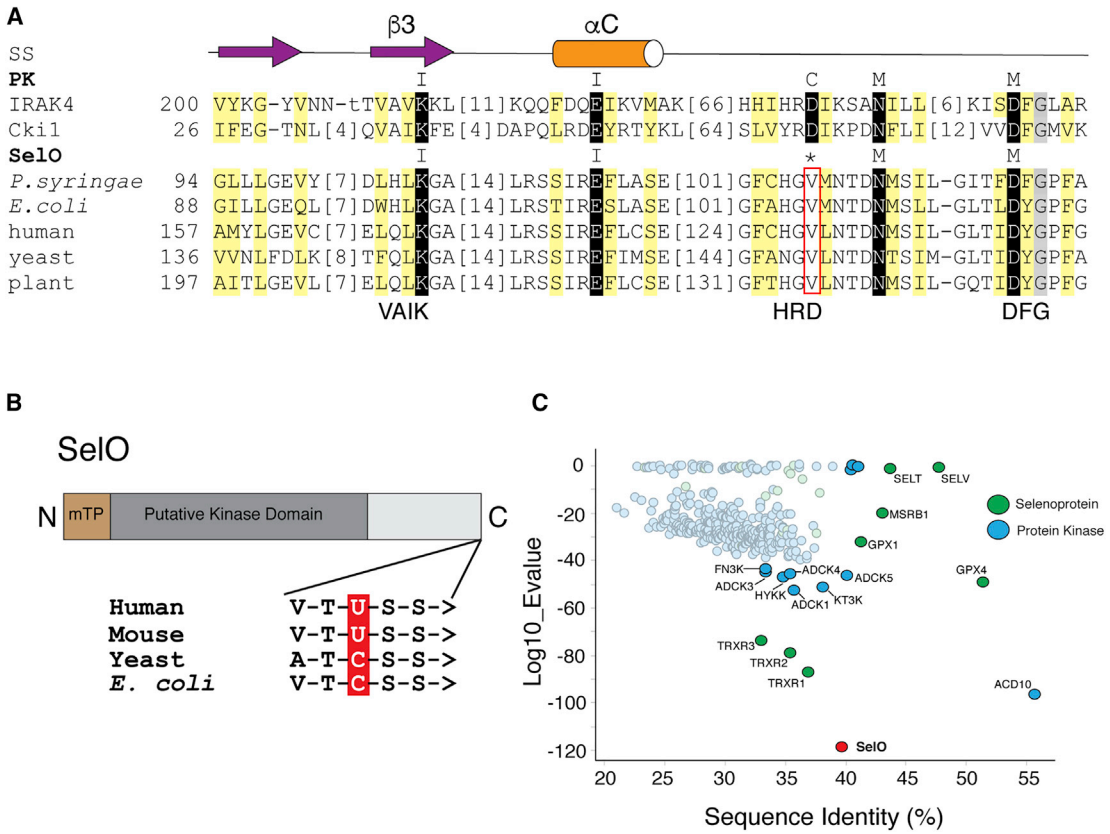

Figure 1. SelO Is an Evolutionarily Conserved Pseudokinase

(A) Multiple sequence alignment highlighting conserved active site residues in the SelO pseudokinases. Conserved positions in SelO and protein kinases (PK) are highlighted yellow (hydrophobic) and gray (small). Conserved catalytic motif residues are highlighted black and labeled above: ion pair (I, VAIK), catalytic (C, HRD), and Mg^{2+} binding (M, DFG). Starting residue numbers are indicated before the alignment, with omitted residue numbers in brackets. Secondary structure (SS) elements are indicated above the alignment as arrow (strand) and cylinder (helix). Cki1, *S. pombe* protein kinase CK1; IRAK4, human interleukin-1 receptor-associated kinase 4. The asterisk denotes the missing catalytic Asp in the SelO pseudokinases.

(B) Schematic representation of the SelO protein depicting the predicted mitochondrial targeting peptide (mTP) and kinase domain. The amino acid sequences at the C terminus of the human, mouse, yeast, and *E. coli* proteins are shown, highlighting the Sec (U) in the human and mouse proteins and Cys (C) in the yeast and *E. coli* proteins. > denotes the C terminus.

(C) BLAST analysis depicting the closest bacterial homologs retrieved from a search using the human protein kinases (blue) and selenoproteins (green) as queries. SelO is in red.

See also Figure S1.

Asp binds the divalent cation to coordinate the β and γ phosphates of ATP (PKA; D184). However, some predicted pseudokinases have evolved compensatory mechanisms to catalyze phosphorylation by migration of active site residues including the WNK family of kinases (Min et al., 2004) and the protein O-mannosyl kinase, SGK196 (Zhu et al., 2016). Such compensatory mutations are often difficult to identify by primary amino acid sequence alone and have resulted in the wrongful annotation of some kinases as inactive.

We previously predicted SelO to adopt a protein kinase fold (Dudkiewicz et al., 2012). However, its sequence suggests that SelO would be an inactive pseudokinase because it lacks the catalytic Asp (PKA; D166) (Figures 1A and S1). Human SelO localizes to the mitochondria and incorporates the 21st genetically encoded amino acid Sec (Han et al., 2014; Kryukov et al., 2003). Structurally, Sec is similar to Cys but contains a selenium atom in place of sulfur (Stadtman, 1974). The resulting selenol group has a lower pKa than the sulfur-containing thiol group and is deprotonated at physiological pH, resulting in higher nucleophilicity and oxidoreductase efficiency (Labunskyy et al., 2014). 25 selenoproteins are encoded in the human genome, and many are involved in cellular redox homeostasis (Kryukov et al., 2003). In higher eukaryotes, most SelO homologs contain a single Sec near the carboxy terminus (Han et al., 2014; Kryukov et al., 2003). In lower eukaryotes and all prokaryotes containing a SelO homolog, an invariant Cys occupies the equivalent position (Figure 1B). For simplicity, we will use the SelO name for the entire family regardless of whether or not the protein contains a Sec.

SelO is highly conserved, having homologs widespread among most eukaryotic taxa, and is also common in many major bacterial taxa (Dudkiewicz et al., 2012). Despite this

sequence-based indicator of a universal role across kingdoms, the molecular function of SelO is unknown. In fact, when prioritizing targets for experimental study, Koonin and colleagues listed SelO among the top ten most-attractive ''unknown unknowns'' because of phyletic spread and potential to reveal new and exciting biology (Galperin and Koonin, 2004).

Here, we report the crystal structure of a SelO homolog, which reveals a protein kinase-like fold. Remarkably, the ATP in the active site is flipped relative to the orientation of ATP in the active site of canonical kinases. Our structural studies led us to discover that the SelO pseudokinases are in fact active enzymes, yet transfer AMP, instead of a phosphate group, to Ser, Thr, and Tyr residues on protein substrates (AMPylation, aka adenylylation). Furthermore, we uncover that SelO plays an evolutionarily conserved role in the cellular response to oxidative stress by AMPylating proteins involved in redox homeostasis. We anticipate that the results of this work will have important implications for redox biology and may have the potential to define new paradigms of cellular regulation and signal transduction.

RESULTS

SelO Is One of the Most Highly Conserved Members of the Protein Kinase and Selenoprotein Families

To demonstrate the unique conservation of SelO, we performed basic local alignment search tool (BLAST) analyses against the Representative Proteomes RP55 database limited to bacteria using known human kinase domains and selenoproteins as queries in the search. We represent conservations of these different kinase and selenoprotein families as a plot of E value versus sequence identity of the top bacterial protein returned from the search (Figure 1C). Our results indicate that SelO is one of the most highly conserved members of either the human protein kinase families or the various selenoprotein families. Among bacteria, SelO is ubiquitous in Proteobacteria and Cyanobacteria, while in other phyla it is less frequent. In eukaryotes, most phyla contain on average 1 *SelO* gene per genome, while chordates and arthropods are exceptions, having an average of 2 or 0.14 genes per genome, respectively.

SelO Adopts a Protein Kinase Fold with ATP Flipped in the Active Site

To gain insight into the function of the SelO pseudokinases, we solved the crystal structure of the SelO homolog from the gram-negative plant pathogen *Pseudomonas syringae* bound to an ATP derivative AMP-PNP (Figures 2A and S2A; Table S1). Despite the unique sequence found in the SelO family, *P. syringae* SelO adopts a protein kinase-like fold consisting of 12 β strands and 22 α helices, with the kinase domain identifying a number of kinase structures as top hits using DALI or VAST structural homology search engines (i.e., aerobactin synthase IucA, the plant receptor kinase BRASSINOSTEROID INSENSITIVE 1, the human interleukin-1 receptor-associated kinase 4, and tyrosine kinase Syk). The kinase core (β4–α14) consists of a β strand-rich N lobe and an α-helical-rich C lobe connected by a flexible linker that can be superimposed onto protein kinase CK1 with a root-mean-square deviation (RMSD) of 3.5 Å over 164 Cα atoms (Figure S2B). The SelO N lobe includes the regulatory αC helix (Figure 2A, orange) packing against the core β sheet (Figure 2A, magenta), while the C lobe includes a pseudo-catalytic loop lacking HRD, followed by an apparent activation loop. An N-terminal extension (α1–α5, white) stabilizes the N lobe β sheet, and the unique C-terminal domains, CTD1 (α15–α19) and CTD2 (α20–α22), contact the C lobe and the αC helix, respectively. There is no clear electron density for the last 12 residues, including the C-terminal Cys, suggesting that this region is disordered.

The SelO nucleotide sits in a cleft between the two lobes of the kinase domain. Remarkably, the AMP-PNP molecule is flipped in the active site when compared to canonical protein kinases. The γ-phosphate, which is normally transferred to protein in a kinase reaction, is buried in a pocket between the two lobes of the kinase domain (Figure 2B). In fact, after superposition of the kinase domains, the SelO α-, β-, and γ-phosphates occupy the positions of the typical γ-, β-, and α-phosphates of protein kinases, respectively (Figures 2B, 2C, and S2C). The binding site for the flipped nucleotide adenine base and sugar ribose is formed by unique insertions in two SelO loops: the β6–β7 (Gly-rich loop) and the β8-αC loop (colored white, Figures 2B and 2D).

SelO Transfers AMP from ATP to Protein Substrates

The flipped orientation of ATP in the active site led us to hypothesize that the SelO proteins could transfer adenosine monophosphate (AMP) to protein substrates (AMPylation) (Casey and Orth, 2018). We incubated recombinant *E. coli* (ydiU), *S. cerevisiae* (Fmp40), and *H. sapiens* SelO with [γ^{32}P]ATP or [α^{32}P]ATP of similar specific radioactivity and observed ^{32}P-incorporation into the wild-type (WT) proteins only when [α^{32}P]ATP was used as substrate (Figures 3A–3C). Mutation of the active site metal-binding DFG motif in the SelO proteins abolished ^{32}P incorporation. *E. coli* and human SelO, but not the inactive mutants, were immunoreactive to an anti-Thr AMP antibody (Figures S3A and S3B) (Hao et al., 2011). Likewise, mass spectrometry (MS) analysis revealed peptides from WT SelO proteins but not the inactive mutants, with mass shifts of 329 Da, consistent with the covalent addition of AMP to Ser, Thr, and Tyr residues (Figures 3D and S3C). Furthermore, *E. coli* SelO, but not the inactive mutant, could AMPylate the generic protein kinase substrate myelin basic protein (MBP) in a time-dependent manner (Figure 3E). *E. coli* SelO prefers ATP over other nucleotides as a co-substrate (Figure S3D) and displayed a K_m for ATP of ~2.0 μM (Figure S3E). Thus, the SelO pseudokinases can AMPylate protein substrates.

Unique Interactions within the SelO Active Site Facilitate Nucleotide Binding and AMPylation

Several interactions within the SelO active site contribute to the inverted orientation of the nucleotide, including K113 (PKA; K72) that coordinates the γ-phosphate of ATP (Figure 4A). K113 extends into the active site and is stabilized by E136 from the α6/αC helix. The formation of this ion pair, which typically positions the α-phosphate of ATP, is considered a hallmark of the activated state of a protein kinase (Taylor and Kornev, 2011). Two invariant arginines (R176 and R183) also form interactions with the γ-phosphate. R176 extends into the active site from

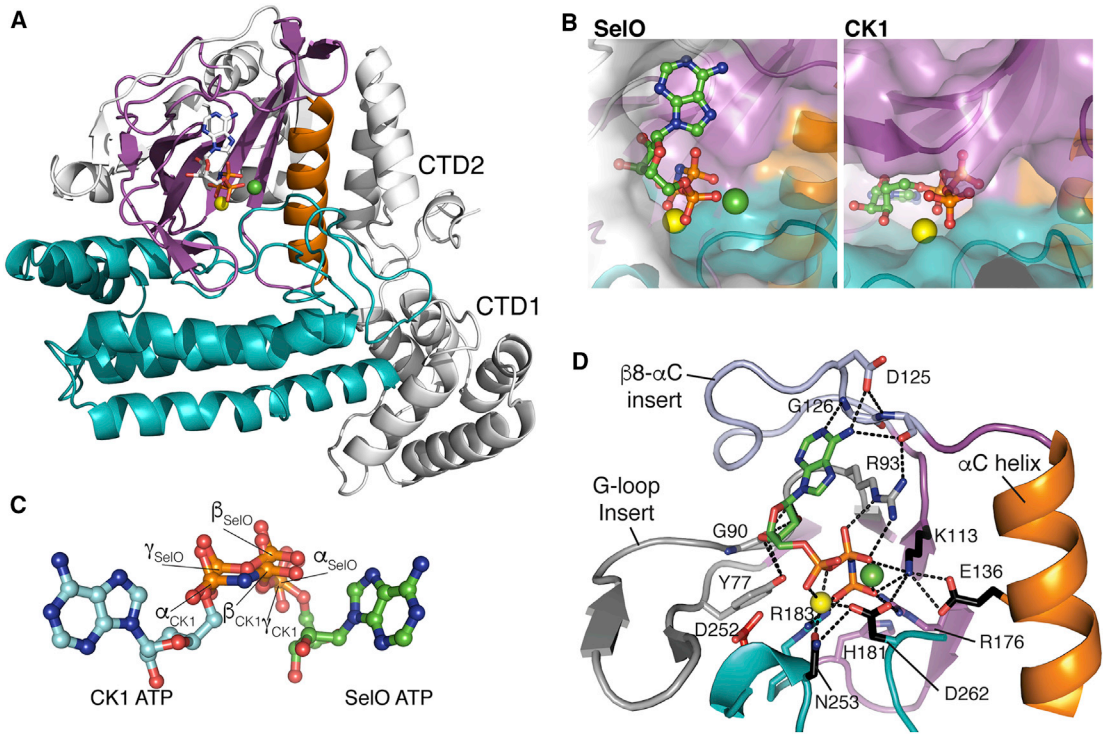

Figure 2. The Crystal Structure of *P. syringae* SelO Reveals an Atypical Protein Kinase Fold with ATP Flipped in the Active Site

(A) Ribbon representation of *P. syringae* SelO. The N and C lobes are shown in magenta and teal, respectively. The αC helix is in orange. The N-terminal extension and C-terminal domains are in white. The AMP-PNP is shown in stick representation, and the Mg^{2+} and Ca^{2+} ions are shown as yellow and green spheres, respectively.

(B) Surface representations illustrating the orientation of the nucleotide in the active site of *P. syringae* SelO (left), colored as above, but with N lobe insertions shown in white and protein kinase CK1 (right, pdb: 1csn) in the same orientation as SelO.

(C) Ball-and-stick representation of SelO and CK1 nucleotides superimposed as a result of superposition of the proteins. The α-, β-, and γ-phosphates of SelO and CK1 are highlighted.

(D) Enlarged image of the nucleotide-binding pocket of *P. syringae* SelO highlighting the flipped ATP-binding pocket. Two unique SelO insertions bind the flipped nucleotide, including a G90 and Y77 from the elongated G loop (gray) that form hydrogen bonds (black dotted lines) with the ribose ring and R93 that forms hydrogen bonds with the β-phosphate, as well as D125 and G126 from the β8-αC insert (light blue) forming hydrogen bonds with the nucleotide. Two Arg side chains (R176 and R183) form a unique charged pocket for the γ-phosphate, with the side chains from R183 and H181 replacing the canonical ATP nucleotide-binding site.

See also Figure S2 and Table S1.

β12 and R183 lies in the flexible hinge region that connects the N lobe to the C lobe (Figure 4A). Mutations of K113, E136, R176, or R183 to Ala inactivate *E. coli* SelO (Figure 4B). Most kinases require a divalent cation to orient the phosphates of ATP. In the *P. syringae* SelO structure, Mg^{2+} and Ca^{2+} are bound to the α- and β-phosphates of AMP-PNP and are coordinated by N253 and D262 (PKA; N171 and D184). Mutations of these residues to Ala abolished *E. coli* SelO activity (Figure 4B). SelO was predicted to be a pseudokinase because it lacks the catalytic Asp (PKA; D166), which deprotonates the phosphoacceptor hydroxyl on the protein substrate. However, we anticipate that D252 in *P. syringae* SelO could fulfill this role because of its conservation and its proximity to the α-phosphate of ATP. Furthermore, its mutation to Ala inactives *E. coli* SelO (Figure 4B). Collectively, the active site of *P. syringae* SelO reveals evolutionarily conserved interactions that provide this family of kinases with the unique ability to transfer AMP to protein substrates.

SelO Is a Redox Active Mitochondrial Protein

The N terminus of eukaryotic SelO proteins contains a predicted mitochondrial targeting peptide (mTP). When overexpressed in mammalian cells as a GFP-fusion protein, human SelO localizes to the mitochondria (Han et al., 2014). We expressed *S. cerevisiae* SelO (official gene name *Fmp40*) in yeast as a C-terminally tagged GFP-fusion protein and observed co-localization with the mitochondrial resident protein citrate synthase (Figure S4A). Mitochondrial localization was dependent on the presence of the mTP (residues 1–23) because a truncated mutant of SelO failed to localize to the mitochondria (Figure S4A). Furthermore, we fractionated yeast extracts by sucrose-gradient centrifugation and detected endogenous SelO in fractions enriched for the mitochondrial resident protein porin (Figure S4B). Thus, *S. cerevisiae* SelO is a mitochondrial protein, and its localization depends on a functional mTP.

Many mitochondrial proteins are subjected to redox regulation, including several selenoproteins. To test the redox

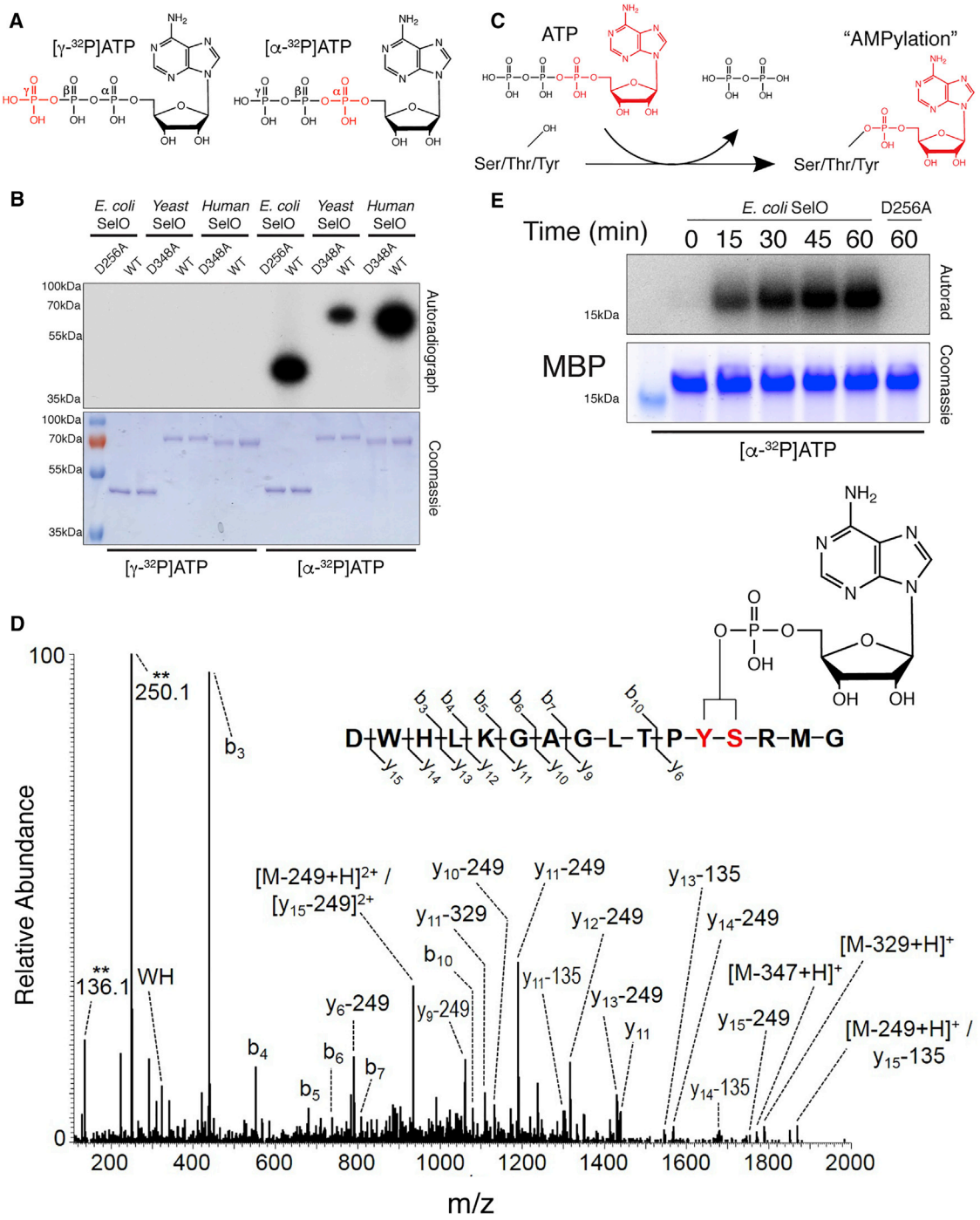

Figure 3. SelO Pseudokinases AMPylate Protein Substrates

(A) Structure of the ATP molecule highlighting the position of the ^{32}P on the γ-phosphate (left) or α-phosphate (right) in red.

(B) Autoradiograph depicting the incorporation of γ-^{32}P from [γ-^{32}P]ATP (left) or α-^{32}P from [α-^{32}P]ATP (right) using *E. coli*, *S. cerevisiae*, and human SelO (U667C) or catalytically inactive mutants. Reaction products were resolved by SDS-PAGE and visualized by Coomassie blue staining (lower) and autoradiography (upper).

(C) Proposed reaction catalyzed by the SelO pseudokinases.

(D) MS/MS spectrum of an AMPylated *E. coli* SelO peptide ion generated by Asp-N digestion. The precursor ion, *m/z* 1059.47 (2+), of the AMPylated peptide was subjected to HCD fragmentation to generate the spectrum shown. Fragment ions containing the modified residue show characteristic mass shifts corresponding to loss of the AMP group (−329, −249, and −135 Da). Unique ions corresponding to neutral loss of the AMP group (labeled with **) are present at 136.1 and 250.1 Da. Location of the AMP group on the peptide can be localized to either the tyrosine or serine residue highlighted in red.

(E) Time-dependent incorporation of α-^{32}P from [α-^{32}P]ATP into MBP by SelO or SelO D256A. Reaction products were analyzed as in (B).

See also Figure S3.

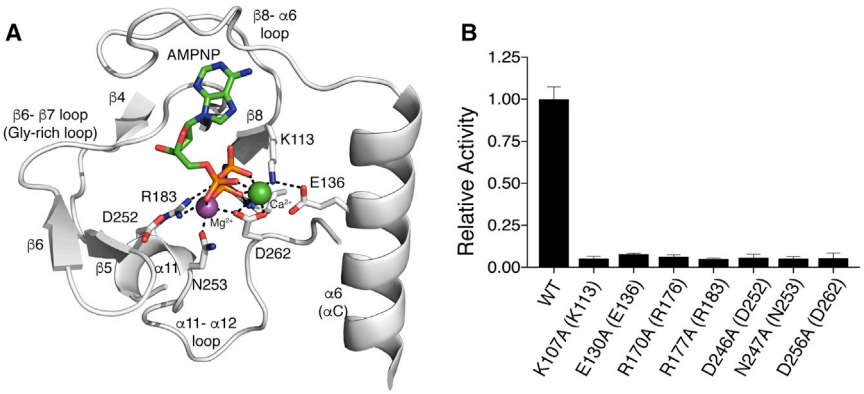

Figure 4. A Unique Active Site Architecture in *P. syringae* SelO Facilitates ATP Binding and AMPylation Activity

(A) Enlarged image of the nucleotide-binding pocket of *P. syringae* SelO showing the detailed molecular interactions important for nucleotide binding and catalysis. Interactions are shown as dashed lines. The AMP-PNP molecule is shown in stick, and the Mg^{2+} and Ca^{2+} ions are shown as purple and green spheres, respectively.

(B) Activity of *E. coli* SelO or active site mutants using MBP and [α-^{32}P]ATP as substrates. Reaction products were resolved by SDS-PAGE, and radioactive gel bands were excised and quantified by scintillation counting. The numbering in parentheses corresponds to the residues in *P. syringae* SelO.

See also Figure S7.

function of SelO, we purified the *E. coli* protein under non-reducing conditions and observed a doublet when the protein was resolved by non-reducing SDS-PAGE (Figure 5A). The faster migrating species was converted to the slower migrating species upon treatment with the reducing agent dithiothreitol (DTT). Likewise, endogenous *S. cerevisiae* SelO migrated as two distinct species during non-reducing SDS-PAGE and was also sensitive to DTT (Figure 5B). MS analysis of *E. coli* SelO identified an intramolecular disulfide bond between Cys272 and Cys476 (Figure 5C). To confirm the sites of modification, we incubated *E. coli* SelO with the cysteine alkylating agent 4-acetamido-4′-maleimidylstilbene-2,2′-disulfonic acid (AMS). AMS reacts with free thiols, resulting in a change in electrophoretic mobility that can be easily observed by SDS-PAGE. AMS reduced the electrophoretic mobility of WT SelO only in the presence of the reducing agent, Tris(2-carboxyethyl) phosphine (TCEP). However, AMS reduced the electrophoretic mobility of the C272A and C476A mutants in the absence of TCEP (Figure 5D). Collectively, these results suggest that *E. coli* SelO forms an intramolecular disulfide bond between a Cys in the activation loop and the Cys at the C terminus, the latter being replaced by a Sec in higher eukaryotes (Figures 1B and 5E).

The formation of disulfide bonds occurs primarily in the oxidizing environment of the secretory pathway. However, some mitochondrial proteins can also form disulfide or selenylsulfide bonds as part of their catalytic mechanism (Collet and Messens, 2010). To test whether the SelO disulfide bond regulates its activity, we incubated *E. coli* SelO purified under non-reducing conditions, with MBP and [α^{32}P]ATP, and observed low levels of AMPylation (Figure 5F). However, addition of DTT or the thioredoxin system that uses reducing equivalents from nicotinamide adenine dinucleotide phosphate (NADPH) to reduce disulfides markedly increased SelO activity. Therefore, *E. coli* SelO activity is regulated by the formation of an intramolecular disulfide bridge.

SelO AMPylates Proteins Involved in Redox Biology

Based on the chemistry of the AMPylation reaction and the location of the adenine ring of ATP in the SelO crystal structure, we reasoned that using a biotinylated ATP analog would be an efficient strategy to identify proteins AMPylated by SelO. In this reaction, biotinylated AMP would be transferred to proteins, which would greatly facilitate isolation and identification of SelO substrates. We incubated *E. coli* SelO with biotin-17-ATP (Figure 6A) and *E. coli* extracts (Figure 6B). Remarkably, several biotinylated proteins were observed in extracts incubated with WT SelO but not the inactive mutant. To identify SelO targets, we enriched biotinylated proteins by avidin pulldown and identified potential SelO substrates by MS, several of which have roles in oxidative phosphorylation and redox biology (Table S2). Among our top candidates are sucA, the bacterial homolog of the E1 component of the α-ketoglutarate dehydrogenase complex (Frank et al., 2007) and glutaredoxin (grx), a small thioredoxin-like protein that catalyzes the removal of covalently linked glutathione from Cys residues on proteins (deglutathionylation) (Shelton et al., 2005).

To test whether *E. coli* sucA and grxA are AMPylated by SelO in cells, we co-expressed *E. coli* SelO or the inactive mutant with His-tagged sucA or grxA and analyzed Ni-NTA-affinity-purified proteins for AMPylation by MS. We identified AMPylated tryptic peptides on sucA and grxA that were present when co-expressed with WT but not inactive SelO (Figure S5). Notably, we identified Thr405 on sucA and Tyr13 on grxA to be potential sites of modification. Protein immunoblotting of sucA using an anti-Thr AMP antibody confirmed that Thr405 was the major site of AMPylation (Figure 6C). Likewise, SelO AMPylated WT grxA *in vitro* but not the Y13F mutant (Figure 6D). Thus, SelO can AMPylate Thr and Tyr residues on protein substrates both *in vitro* and *in vivo*.

To determine the substrate specificity of SelO, we performed AMPylation reactions using *E. coli* grxA as a model substrate. Alanine substitutions of the Cys at the −2 and Pro at the −1 positions, or replacing the AMP-acceptor Tyr with a Ser or a Thr, markedly inhibited SelO-mediated AMPylation (Figure S6A). However, analysis of the auto AMPylation sites in *E. coli*, yeast, and human SelO (Figure S3C), and the grxA and sucA sites (Figure S5), did not reveal any obvious primary sequence requirements for SelO-catalyzed AMPylation. Therefore, SelO appears to require additional factors beyond the primary amino acid sequence of the substrate.

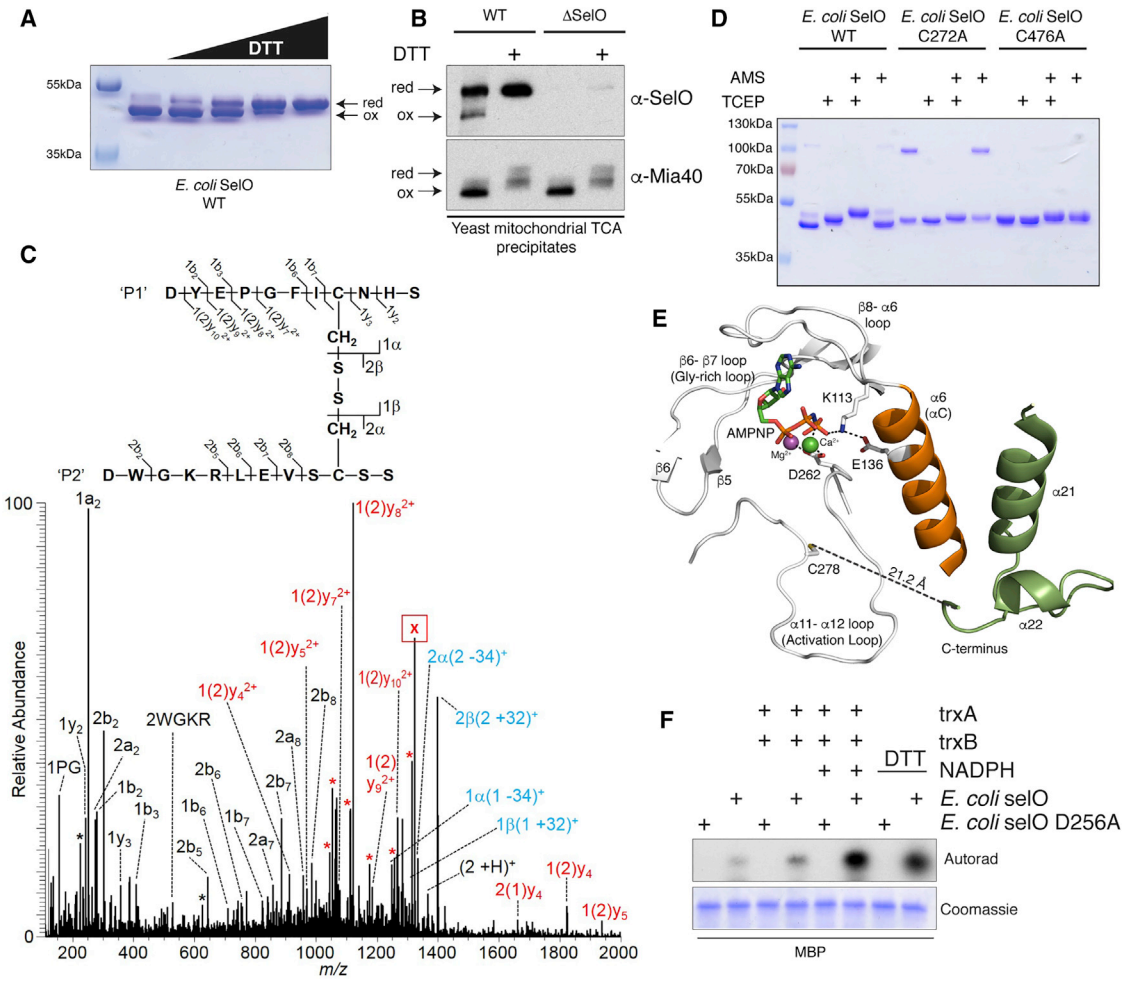

Figure 5. SelO Activity Is Regulated by an Intramolecular Disulfide Bridge

(A) Non-reducing SDS-PAGE and Coomassie blue staining analysis of recombinant *E. coli* SelO purified in the absence of reducing agent and incubated with increasing concentrations of DTT (0–1 mM).

(B) Non-reducing SDS-PAGE and protein immunoblotting of yeast mitochondrial TCA precipitates depicting endogenous *S. cerevisiae* SelO and Mia40. TCA precipitates were treated with or without DTT prior to electrophoresis.

(C) MS/MS spectrum of *E. coli* SelO peptides linked by a disulfide bond: DYEPGFICNHS / DWGKRLEVSCSS. The precursor ion, *m/z* 1323.07 (2+) (labeled with "X"), was subjected to HCD fragmentation to generate the spectrum shown. Peaks labeled with an asterisk (*) correspond to neutral loss of ammonia (−17 Da) or water (−18 Da) from fragment ions. The peak labels are color coded depending on the status of the disulfide bond (SS) for that particular ion: black, no SS; red, intact SS; and blue, asymmetric cleavage of SS, α, or β.

(D) Non-reducing SDS-PAGE and Coomassie blue staining analysis of recombinant *E. coli* SelO or the C272A and C476A mutants purified under non-reducing conditions and incubated with the reducing agent TCEP or the alkylating agent AMS. The species at ~100 kDa in the SelO C272A mutant is a dimer formed between two molecules of *E. coli* SelO linked by an intermolecular disulfide.

(E) Enlarged image of the active site highlighting the activation loop C278 (C272 in *E. coli* SelO) and the C terminus of the protein. The α6 (αC equivalent) is in orange, and the α21 and α22 helices are in green. The AMP-PNP molecule is shown in stick, and the Mg^{2+} and Ca^{2+} ions are shown as purple and green spheres, respectively.

(F) Incorporation of ^{32}P AMP from [α-^{32}P]ATP by *E. coli* SelO or the D256A mutant under non-reducing or reducing conditions (DTT or the thioredoxin system). trxA, *E. coli* thioredoxin; trxB, *E. coli* thioredoxin reductase. Reaction products were analyzed as in Figure 3B.

See also Figure S4.

SelO-Mediated AMPylation Protects *S. cerevisiae* from Oxidative Stress

The substrates identified from the biotin pulldown experiments and the fact that Sec-containing proteins are typically involved in redox homeostasis led us to hypothesize that SelO is involved in the cellular response to oxidative stress. Yeast grown on non-fermentable carbon sources induce oxidative stress through mitochondrial respiration (Farrugia and Balzan, 2012; Grant et al., 1997). We detected an increase in *S. cerevisiae* SelO protein levels in cells grown on the non-fermentable carbon sources glycerol, lactate, and acetate (Figure 7A). These results are consistent with previous studies showing that yeast SelO mRNA expression correlates with the stress response and is induced in respiring cells (Tu et al., 2005).

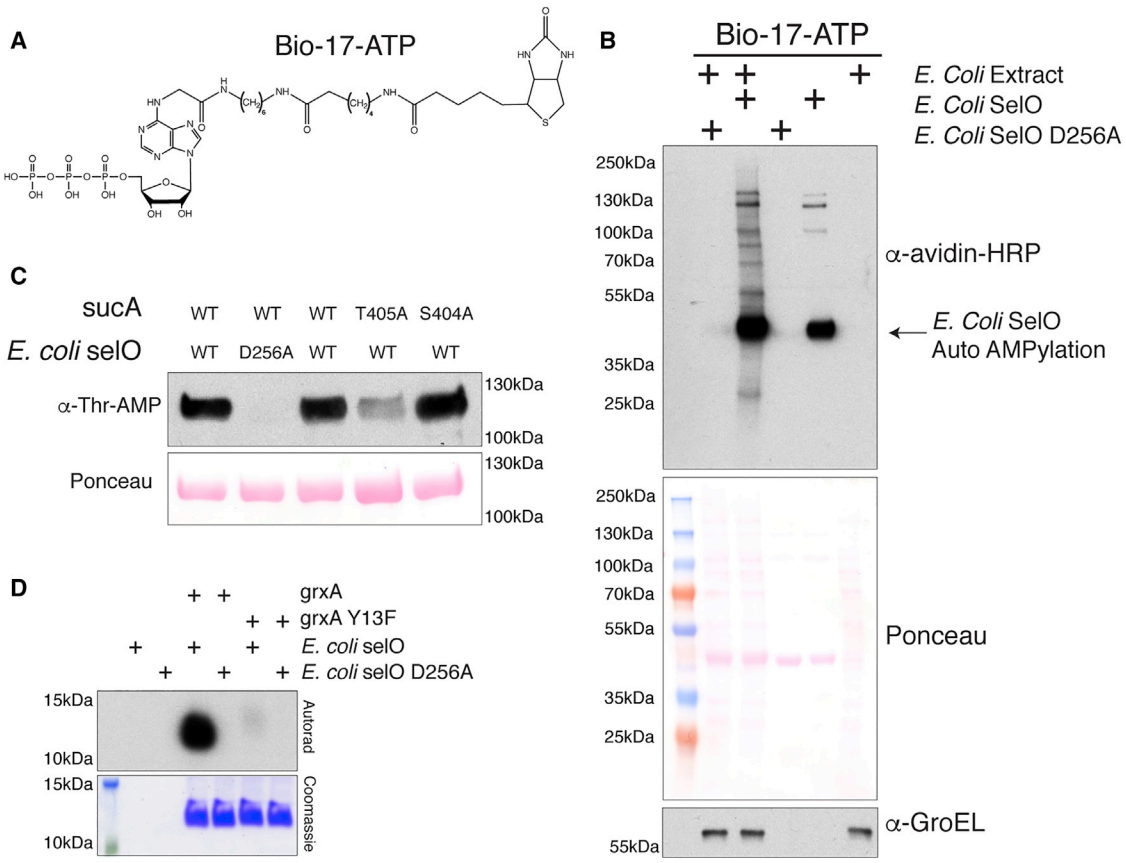

Figure 6. SelO AMPylates Redox Proteins

(A) Structure of biotin-17-ATP (bio-17-ATP) used in these experiments to identify SelO substrates.

(B) Representative blot using avidin-HRP to detect biotinylated proteins following incubation of *E. coli* extracts with bio-17-ATP and *E. coli* SelO or the D256A mutant. The Ponceau stained membrane and an immunoblot for GroEL are shown as loading controls.

(C) α-Thr AMP protein immunoblotting of Ni-NTA affinity purified His-tagged sucA (or mutants) from SelO KO *E.coli* extracts expressing untagged WT SelO or the inactive mutant. The Ponceau stained membrane is shown.

(D) Autoradiograph depicting the incorporation of α-^{32}P AMP from [α-^{32}P]ATP by *E. coli* SelO or the D256A mutant into *E. coli* grxA. Reaction products were analyzed as in Figure 3B.

See also Figure S5 and Table S2.

We challenged WT and SelO-deficient *S. cerevisiae* with H_2O_2 and observed a decrease in survival in SelO knockout (KO) cells (Figure 7B). Cell viability was fully complemented by WT SelO but not the inactive mutant. We then incubated WT and SelO KO yeast with the redox-cycling compound menadione, which increases cellular reactive oxygen species (Zadziński et al., 1998). SelO-deficient yeast displayed a menadione-dependent growth defect that was fully rescued by WT *S. cerevisiae* SelO but not the catalytically inactive mutant (Figure 7C). Collectively, these results suggest that SelO-mediated AMPylation of proteins protects *S. cerevisiae* from oxidative stress.

SelO Regulates Global S-glutathionylation Levels in Bacteria and Yeast

The reversible oxidative modification of cysteine residues on proteins with a molecule of glutathione (S-glutathionylation) is emerging as a ubiquitous and essential mechanism for protecting proteins exposed to oxidative conditions (Figure S6B) (Mieyal and Chock, 2012). Under oxidative stress, protein thiols can become reversibly oxidized to sulfenic acids that are protected from over-oxidation by S-glutathionylation. Protein S-glutathionylation is reversed by the grx family of deglutathionylation enzymes, which form a mixed disulfide intermediate to restore the free thiol on target proteins (Shelton et al., 2005). Interestingly, Tyr13 in *E. coli* grxA, which is AMPylated by SelO, lies within the highly conserved redox active site of the enzyme (^{11}C-P-Y-C^{14}) and interacts with glutathione (Figures S6C and S6D). Therefore, we hypothesized that SelO-mediated AMPylation of grx family members would regulate S-glutathionylation of proteins *in vivo*. Under normal growth conditions, SelO deficient *E. coli* and yeast showed a modest decrease in global S-glutathionylation as judged by protein immunoblotting using a S-glutathionylation specific antibody (Figures 7D and 7E, respectively; lanes 1 and 2). However, when cells were treated with oxidized glutathione (GSSG) or diamide, conditions known to increase protein S-glutathionylation (Ghezzi et al., 2002; Sun et al.,

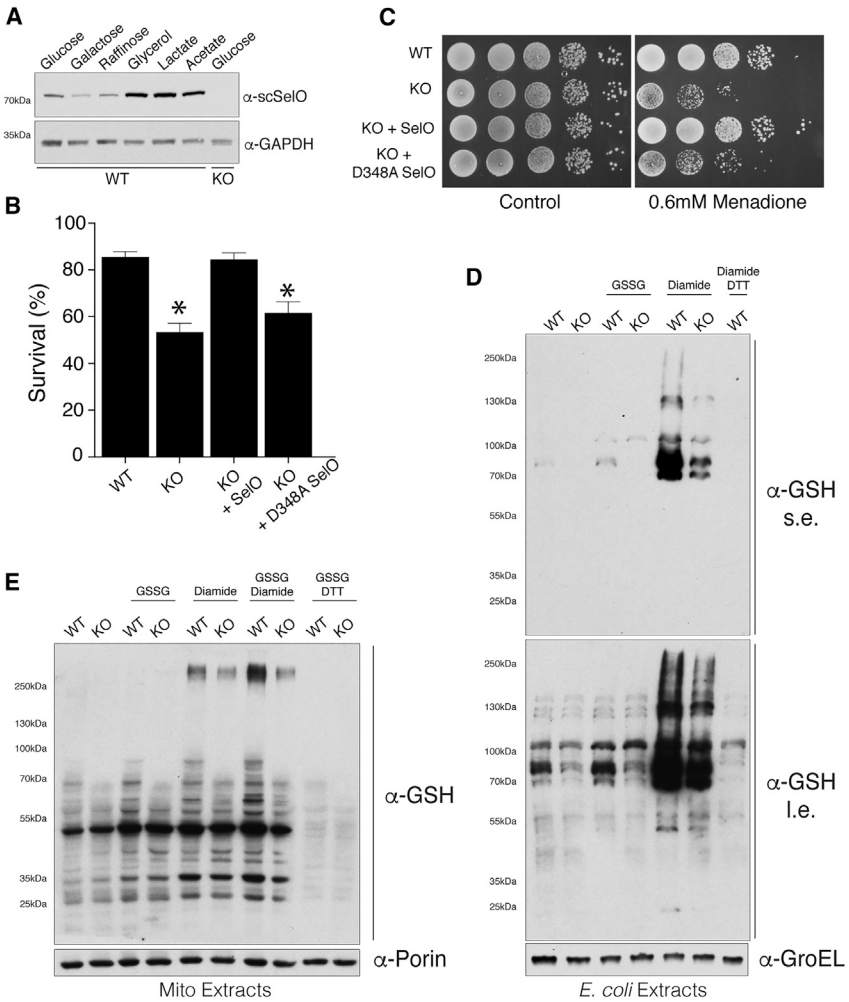

Figure 7. SelO Protects Yeast Cells from Oxidative Stress and Regulates Protein S-glutathionylation

(A) Representative protein immunoblots of WT and SelO KO yeast cell extracts (strain MR6) grown in medium with the indicated carbon source. *S. cerevisiae* SelO (ScSelO) and GAPDH (loading control) are shown.

(B) Percent survival of *S. cerevisiae* (strain MR6) WT, SelO KO, or SelO KO cells complemented with WT or D348A SelO following treatment with 100 μM H_2O_2 in glucose minimal medium for 200 min at 28°C. Results represent the mean of 3 independent experiments. *$p < 0.005$ versus WT.

(C) Representative growth assays of *S. cerevisiae* (strain BY4741) untreated (left) or 0.6 mM menadione treated (right). WT, SelO KO, or SelO KO complemented with WT or D348A SelO strains were analyzed.

(D) Representative protein immunoblots of WT and SelO KO *E. coli* extracts following treatment of intact cells with oxidized glutathione (GSSG) or diamide. Cells were also treated with diamide followed by DTT as a negative control. Extracts were probed with anti-glutathionylation (GSH) and *E. coli* GroEL (loading control). Results are representative of at least 3 independent experiments. s.e., short exposure; l.e., long exposure.

(E) Representative protein immunoblots of crude mitochondrial extracts isolated from WT and SelO KO *S. cerevisiae* (strain MR6) following treatment of intact mitochondria with oxidized glutathione (GSSG) and/or diamide. Mitochondria were also treated with GSSG followed by DTT as a negative control. Extracts were probed with anti-glutathionylation (GSH) and *S. cerevisiae* porin (loading control). Results are representative of at least 3 independent experiments.

See also Figure S6.

2012), we observed a marked decrease in S-glutathionylation levels in both bacterial and yeast SelO KO cells (Figures 7D and 7E, respectively; lanes 4-7). Collectively, these results suggest that SelO regulates protein S-glutathionylation levels by AMPylation of the grx family of enzymes.

DISCUSSION

Our structural analysis of *P. syringae* SelO has unexpectedly discovered a previously unrecognized activity for a member of the protein kinase superfamily. There are other enzymes in nature that can AMPylate protein substrates on amino acid side chains, including glutamine synthase adenylyltransferase (GS ATase) (Shapiro and Stadtman, 1968), the Legionella effector DrrA/SidM (Müller et al., 2010), and proteins containing the Fic domain (Worby et al., 2009; Yarbrough et al., 2009). However, SelO is unique because it has a protein kinase fold. GS ATase and DrrA adopt an α+β nucleotidyltransferase fold and catalyze AMPylation using a conserved G-X_{11}-D-X-D motif (Holm and Sander, 1995). In DrrA, the second Asp of the motif acts as a general base to deprotonate the protein substrate Tyr, which then acts as a nucleophile on the α-phosphate of ATP (Gavriljuk et al., 2014). Fic family proteins adopt a mainly α-helical bundle fold with a conserved H-X-F-X-(D/E)-(A/G)-N-(G/K)-R motif (Kinch et al., 2009; Xiao et al., 2010). The Fic motif His residue acts as the general base in catalysis, while the Arg positions the β-phosphate and stabilizes the developing negative charge on the α-phosphate during catalysis (Luong et al., 2010). A second Arg just upstream of the Fic motif forms a hydrogen bond with the γ-phosphate of the bound nucleotide. Interestingly, the Fic-related Doc toxin is thought to use inverted ATP to phosphorylate protein substrates (Castro-Roa et al., 2013). Analogous to the Fic and Doc proteins, our results suggest that a flip of the ATP in protein kinases allows the switch between AMPylation and phosphorylation of protein substrates.

In each of the known folds capable of catalyzing AMPylation, a key conserved residue acts as a general base to deprotonate the protein target Tyr or Thr residue. Sequence conservation of the SelO active site suggests that the catalytic Asp that performs this function (D252 in *P. syringae* SelO) has migrated from the canonical position in traditional protein kinases. Accordingly, mutagenesis supports a critical role for this residue in catalysis

(Figure 4B). To gain understanding of the potential SelO peptide-binding site, we superimposed the SelO kinase domain with activated FGFR2 kinase bound to a peptide substrate (Figure S7A) (Chen et al., 2007). The canonical protein kinase active site Asp (PKA; D166) approaches the substrate Tyr OH from one side, while the migrated SelO active site Asp approaches from the opposite side. A Pro residue at the C terminus of the FGFR2 activation loop that positions the substrate peptide Tyr is replaced by a conserved aromatic residue (F82) from the SelO Gly-rich loop insert. Two additional SelO family conserved residues from the Gly-rich loop insert (Q81) and the β8-αC insert (R122) that define the flipped ATP site, might also contribute to an extended SelO peptide substrate binding site.

The SelO C-terminal domains (CTDs) bridge the regulatory αC helix with the activation loop and position the αC helix in the active conformation. This interaction resembles the activation of cyclin-dependent kinase CDK2 by cyclin A (Jeffrey et al., 1995). The CDK2 regulatory αC helix PSTAIRE motif retains a conserved RE (PKA; E91) in the same position as the invariant RE from SelO (Figures S7B and S7C). The Arg residues from both kinases form key hydrogen bond interactions with the activation loops, while the Glu residues form an ion pair with their corresponding Lys (PKA; K72) marking the activated state of the protein kinase. In the absence of cyclin, the αC helix and the activation loop of free CDK2 adopt alternate conformations, rendering the kinase inactive. The free CDK2 regulatory helix rotates away from the active site pocket, disrupting residues involved in orienting phosphate and coordinating Mg^{2+}. The free CDK2 activation loop covers the active site and prevents ATP access. The SelO CTD2 prevents such a rotation of the regulatory αC helix in the present SelO structure. The disordered C terminus extending from CTD2 plays a role in inactivating the kinase by forming a disulfide bond with a Cys in the activation loop. Analogous to CDK2, this inactivation could involve a conformational change of the CTD to allow rotation of the regulatory αC helix or an alternate conformation of the activation loop driven by disulfide bond formation, or both.

Interestingly, in the crystal structure of *P. syringae* SelO, the conserved activation loop cysteine (C279, corresponding to C272 of *E. coli* SelO) is in a position compatible with formation of a disulfide bond with another cysteine, C246 (the Cβ-Cβ distance is 3.8 Å). The C246 (not present in *E. coli* SelO) is located only seven residues away from the predicted catalytic D252. Thus, the regulatory mechanism of intramolecular disulfidebond formation may be more complex in some members of the SelO family possessing more than one cysteine in the activation loop or in the catalytic loop. Future work will be needed to confirm the physiological importance of the selenylsulfide or disulfide bond and its role in regulating AMPylation activity of SelO from different species.

We have developed a strategy using a biotinylated ATP derivative to identify SelO substrates. Notably, we identified the glutaredoxins and the E1 component of the α-ketoglutarate dehydrogenase complex, sucA, to be direct substrates of *E. coli* SelO. SucA is a component of the 2-oxoglutarate dehydrogenase complex, which catalyzes a rate-limiting step of the tricarboxylic acid cycle (TCA) and is thought to be a mitochondrial redox sensor (McLain et al., 2011). Glutaredoxin is a small redox protein involved in reducing cellular disulfides and removes glutathione from Cys residues on proteins (Shelton et al., 2005). Interestingly, grxA is AMPylated on a highly conserved active site residue, suggesting that AMPylation may regulate its activity (Figures S6C and S6D). Indeed, total protein S-glutathionylation levels were decreased in SelO deficient *E. coli* and yeast (Figure 7D), suggesting that AMPylation of the grx family of enzymes is an evolutionarily conserved mechanism to regulate protein S-glutathionylation levels in cells.

Tyr13 on grxA is located adjacent to the glutathione-binding cysteine residue (Figure S6D), and studies have indicated that the aromatic side chain of Tyr13 provides a niche for glutathione binding and subsequent deglutathionylation acitivity (Saaranen et al., 2009). Therefore, AMPylation of Tyr13 may impose steric hinderance for glutathione binding and would inhibit the enzyme. Similar to SelO mutants, yeast glutaredoxin mutants are more sensitive to oxidative stress induced by menadione and hydrogen peroxide treatment (Luikenhuis et al., 1998). In the case of sucA, Thr405 lies within a disordered loop in the dimerization interface (Figures S6E and S6F). The loop is connected to the active site that coordinates Mg^{2+} (Frank et al., 2007; Wagner et al., 2011). Studies are underway to determine whether AMPylation of sucA regulates the formation of the α-ketoglutarate dehydrogenase complex and/or affects its activity. Collectively, the highly conserved SelO sequence, AMPylation sites in substrates (grxA, sucA), and enzymatic activity suggest that SelO regulates an ancient, conserved oxidative stress defense mechanism in prokaryotes and eukaryotes.

In higher eukaryotes, SelO homologs contain a Sec, whereas a Cys is present in the equivalent position in lower eukaryotes and all prokaryotes with a SelO homolog. Most human selenoproteins have homologs in lower organisms with a Cys in place of the Sec. Incorporation of Sec is energetically expensive; however, the evolutionary advantage of using Sec as opposed to Cys is incompletely understood. Although selenoproteins are considered superior catalysts, it was recently shown that the selenoprotein glutathione peroxidase 4 (GPX4) requires its Sec to prevent irreversible over-oxidation (Ingold et al., 2018). We propose that SelO has evolved a Sec to increase the redox potential of the resulting selenylsulfide bond and/or prevent irreversible over-oxidation, both of which would regulate AMPylation activity.

In summary, we have discovered a new activity for a member of the protein kinase superfamily, which has revealed the molecular function of 1 of the 25 selenoproteins in humans. Our results highlight the structural and biochemical diversity of the protein kinase superfamily and underscore a novel mechanism of redox regulation. Importantly, our results suggest that AMPylation may be more widespread than previously appreciated and that "inactive" kinases should be analyzed for alternative transferase activities.

STAR★METHODS

Detailed methods are provided in the online version of this paper and include the following:

- KEY RESOURCES TABLE
- CONTACT FOR REAGENT AND RESOURCE SHARING
- EXPERIMENTAL MODEL AND SUBJECT DETAILS

SUPPLEMENTAL INFORMATION

Supplemental Information includes seven figures and three tables and can be found with this article online at https://doi.org/10.1016/j.cell.2018.08.046.

ACKNOWLEDGMENTS

We thank Drs. Joseph Goldstein, Eric Olson, Peter Roach, Greg Taylor, Amanda Casey, Benjamin Tu, and members of the Tagliabracci laboratory for insightful discussions. We also thank Christine Nolan and Greg Urquhart for technical assistance. Results shown in this report are derived from work performed at the Argonne National Laboratory, Structural Biology Center at the Advanced Photon Source. This work was supported by NIH grants R00DK099254 (V.S.T.), GM094575 and GM127390 (N.V.G.), GM115188 (K.O.), T32DK007257-37 (A.S.), and T32GM008203-29 (V.A.L.); Welch Foundation grants I-1911 (V.S.T.), I-1505 (N.V.G.), and I-1561 (K.O.); the Once upon a Time…Foundation (K.O.); a CPRIT grant RP170674 (V.S.T.); and the Polish National Science Centre grant 2014/15/B/NZ1/03359 (K.P.). V.S.T. is the Michael L. Rosenberg Scholar in Medical Research, a Cancer Prevention Research Institute of Texas Scholar (RR150033), and a Searle Scholar (SSP-2018-2745).

AUTHOR CONTRIBUTIONS

A.S. and V.S.T. designed the experiments. A.S., S.S.Y., V.A.L., B.C.P., S.P., J.J., M.K.-U., M.L., R.K., D.R.T., and V.S.T. conducted the experiments. J.Z. and K.A.S. performed the mass spectrometry. L.N.K., N.V.G., and K.P. performed the bioinformatics. M.L. and K.O. provided essential reagents. A.S., L.N.K., K.P., and V.S.T. wrote the manuscript with input from all authors.

DECLARATION OF INTERESTS

The authors declare no competing interests.

Received: March 12, 2018
Revised: July 19, 2018
Accepted: August 17, 2018
Published: September 27, 2018

REFERENCES

Adams, P.D., Afonine, P.V., Bunkóczi, G., Chen, V.B., Davis, I.W., Echols, N., Headd, J.J., Hung, L.W., Kapral, G.J., Grosse-Kunstleve, R.W., et al. (2010). PHENIX: a comprehensive Python-based system for macromolecular structure solution. Acta Crystallogr. D Biol. Crystallogr. *66*, 213–221.

Altschul, S.F., Gish, W., Miller, W., Myers, E.W., and Lipman, D.J. (1990). Basic local alignment search tool. J. Mol. Biol. *215*, 403–410.

Altschul, S.F., Madden, T.L., Schäffer, A.A., Zhang, J., Zhang, Z., Miller, W., and Lipman, D.J. (1997). Gapped BLAST and PSI-BLAST: a new generation of protein database search programs. Nucleic Acids Res. *25*, 3389–3402.

Bailey, F.P., Byrne, D.P., McSkimming, D., Kannan, N., and Eyers, P.A. (2015). 2) Going for broke: targeting the human cancer pseudokinome. Biochem. J. *466*, 201.

Borek, D., Cymborowski, M., Machius, M., Minor, W., and Otwinowski, Z. (2010). Diffraction data analysis in the presence of radiation damage. Acta Crystallogr. D Biol. Crystallogr. *66*, 426–436.

Borek, D., Dauter, Z., and Otwinowski, Z. (2013). Identification of patterns in diffraction intensities affected by radiation exposure. J. Synchrotron Radiat. *20*, 37–48.

Borek, D., Minor, W., and Otwinowski, Z. (2003). Measurement errors and their consequences in protein crystallography. Acta Crystallogr. D Biol. Crystallogr. *59*, 2031–2038.

Byrne, D.P., Foulkes, D.M., and Eyers, P.A. (2017). Pseudokinases: update on their functions and evaluation as new drug targets. Future Med. Chem. *9*, 245–265.

Casey, A.K., and Orth, K. (2018). Enzymes Involved in AMPylation and deAMPylation. Chem. Rev. *118*, 1199–1215.

Castro-Roa, D., Garcia-Pino, A., De Gieter, S., van Nuland, N.A.J., Loris, R., and Zenkin, N. (2013). The Fic protein Doc uses an inverted substrate to phosphorylate and inactivate EF-Tu. Nat. Chem. Biol. *9*, 811–817.

Chen, C., Natale, D.A., Finn, R.D., Huang, H., Zhang, J., Wu, C.H., and Mazumder, R. (2011). Representative proteomes: a stable, scalable and unbiased proteome set for sequence analysis and functional annotation. PLoS ONE *6*, e18910.

Chen, H., Ma, J., Li, W., Eliseenkova, A.V., Xu, C., Neubert, T.A., Miller, W.T., and Mohammadi, M. (2007). A molecular brake in the kinase hinge region regulates the activity of receptor tyrosine kinases. Mol. Cell *27*, 717–730.

Chen, V.B., Arendall, W.B., 3rd, Headd, J.J., Keedy, D.A., Immormino, R.M., Kapral, G.J., Murray, L.W., Richardson, J.S., and Richardson, D.C. (2010). MolProbity: all-atom structure validation for macromolecular crystallography. Acta Crystallogr. D Biol. Crystallogr. *66*, 12–21.

Collet, J.F., and Messens, J. (2010). Structure, function, and mechanism of thioredoxin proteins. Antioxid. Redox Signal. *13*, 1205–1216.

Crooks, G.E., Hon, G., Chandonia, J.M., and Brenner, S.E. (2004). WebLogo: a sequence logo generator. Genome Res. *14*, 1188–1190.

Cui, J., Xiao, J., Tagliabracci, V.S., Wen, J., Rahdar, M., and Dixon, J.E. (2015). A secretory kinase complex regulates extracellular protein phosphorylation. eLife *4*, e06120.

Datsenko, K.A., and Wanner, B.L. (2000). One-step inactivation of chromosomal genes in Escherichia coli K-12 using PCR products. Proc. Natl. Acad. Sci. USA *97*, 6640–6645.

Dudkiewicz, M., Lenart, A., and Pawłowski, K. (2013). A novel predicted calcium-regulated kinase family implicated in neurological disorders. PLoS ONE *8*, e66427.

Dudkiewicz, M., Szczepińska, T., Grynberg, M., and Pawłowski, K. (2012). A novel protein kinase-like domain in a selenoprotein, widespread in the tree of life. PLoS ONE *7*, e32138.

Emsley, P., Lohkamp, B., Scott, W.G., and Cowtan, K. (2010). Features and development of Coot. Acta Crystallogr. D Biol. Crystallogr. *66*, 486–501.

Eyers, P.A., and Murphy, J.M. (2013). Dawn of the dead: protein pseudokinases signal new adventures in cell biology. Biochem. Soc. Trans. *41*, 969–974.

Farrugia, G., and Balzan, R. (2012). Oxidative stress and programmed cell death in yeast. Front. Oncol. *2*, 64.

Fedorov, O., Müller, S., and Knapp, S. (2010). The (un)targeted cancer kinome. Nat. Chem. Biol. *6*, 166–169.

Finn, R.D., Clements, J., Arndt, W., Miller, B.L., Wheeler, T.J., Schreiber, F., Bateman, A., and Eddy, S.R. (2015). HMMER web server: 2015 update. Nucleic Acids Res. *43*, W30–W38.

Finn, R.D., Coggill, P., Eberhardt, R.Y., Eddy, S.R., Mistry, J., Mitchell, A.L., Potter, S.C., Punta, M., Qureshi, M., Sangrador-Vegas, A., et al. (2016). The Pfam protein families database: towards a more sustainable future. Nucleic Acids Res. *44* (D1), D279–D285.

Fischer, E.H. (2013). Cellular regulation by protein phosphorylation. Biochem. Biophys. Res. Commun. *430*, 865–867.

Frank, R.A., Price, A.J., Northrop, F.D., Perham, R.N., and Luisi, B.F. (2007). Crystal structure of the E1 component of the Escherichia coli 2-oxoglutarate dehydrogenase multienzyme complex. J. Mol. Biol. *368*, 639–651.

Galperin, M.Y., and Koonin, E.V. (2004). 'Conserved hypothetical' proteins: prioritization of targets for experimental study. Nucleic Acids Res. *32*, 5452–5463.

Gavriljuk, K., Schartner, J., Itzen, A., Goody, R.S., Gerwert, K., and Kötting, C. (2014). Reaction mechanism of adenylyltransferase DrrA from Legionella pneumophila elucidated by time-resolved fourier transform infrared spectroscopy. J. Am. Chem. Soc. *136*, 9338–9345.

Ghezzi, P., Romines, B., Fratelli, M., Eberini, I., Gianazza, E., Casagrande, S., Laragione, T., Mengozzi, M., Herzenberg, L.A., and Herzenberg, L.A. (2002). Protein glutathionylation: coupling and uncoupling of glutathione to protein thiol groups in lymphocytes under oxidative stress and HIV infection. Mol. Immunol. *38*, 773–780.

Grant, C.M., MacIver, F.H., and Dawes, I.W. (1997). Mitochondrial function is required for resistance to oxidative stress in the yeast Saccharomyces cerevisiae. FEBS Lett. *410*, 219–222.

Gregg, C., Kyryakov, P., and Titorenko, V.I. (2009). Purification of mitochondria from yeast cells. J. Vis. Exp. (30), 1417.

Han, S.J., Lee, B.C., Yim, S.H., Gladyshev, V.N., and Lee, S.R. (2014). Characterization of mammalian selenoprotein o: a redox-active mitochondrial protein. PLoS ONE *9*, e95518.

Hao, Y.H., Chuang, T., Ball, H.L., Luong, P., Li, Y., Flores-Saaib, R.D., and Orth, K. (2011). Characterization of a rabbit polyclonal antibody against threonine-AMPylation. J. Biotechnol. *151*, 251–254.

Holm, L., Kääriäinen, S., Rosenström, P., and Schenkel, A. (2008). Searching protein structure databases with DaliLite v.3. Bioinformatics *24*, 2780–2781.

Holm, L., and Rosenström, P. (2010). Dali server: conservation mapping in 3D. Nucleic Acids Res. *38*, W545–W549.

Holm, L., and Sander, C. (1995). DNA polymerase beta belongs to an ancient nucleotidyltransferase superfamily. Trends Biochem. Sci. *20*, 345–347.

Ingold, I., Berndt, C., Schmitt, S., Doll, S., Poschmann, G., Buday, K., Roveri, A., Peng, X., Porto Freitas, F., Seibt, T., et al. (2018). Selenium Utilization by GPX4 Is Required to Prevent Hydroperoxide-Induced Ferroptosis. Cell *172*, 409–422.e21.

Jeffrey, P.D., Russo, A.A., Polyak, K., Gibbs, E., Hurwitz, J., Massagué, J., and Pavletich, N.P. (1995). Mechanism of CDK activation revealed by the structure of a cyclinA-CDK2 complex. Nature *376*, 313–320.

Jura, N., Shan, Y., Cao, X., Shaw, D.E., and Kuriyan, J. (2009). Structural analysis of the catalytically inactive kinase domain of the human EGF receptor 3. Proc. Natl. Acad. Sci. USA *106*, 21608–21613.

Katoh, K., and Standley, D.M. (2013). MAFFT multiple sequence alignment software version 7: improvements in performance and usability. Mol. Biol. Evol. *30*, 772–780.

Kent, U.M. (1999). Purification of antibodies using ammonium sulfate fractionation or gel filtration. Methods Mol. Biol. *115*, 11–18.

Kinch, L.N., Yarbrough, M.L., Orth, K., and Grishin, N.V. (2009). Fido, a novel AMPylation domain common to fic, doc, and AvrB. PLoS ONE *4*, e5818.

Kryukov, G.V., Castellano, S., Novoselov, S.V., Lobanov, A.V., Zehtab, O., Guigó, R., and Gladyshev, V.N. (2003). Characterization of mammalian selenoproteomes. Science *300*, 1439–1443.

Kung, J.E., and Jura, N. (2016). Structural Basis for the Non-catalytic Functions of Protein Kinases. Structure *24*, 7–24.

Labunskyy, V.M., Hatfield, D.L., and Gladyshev, V.N. (2014). Selenoproteins: molecular pathways and physiological roles. Physiol. Rev. *94*, 739–777.

Longtine, M.S., McKenzie, A., 3rd, Demarini, D.J., Shah, N.G., Wach, A., Brachat, A., Philippsen, P., and Pringle, J.R. (1998). Additional modules for versatile and economical PCR-based gene deletion and modification in Saccharomyces cerevisiae. Yeast *14*, 953–961.

Luikenhuis, S., Perrone, G., Dawes, I.W., and Grant, C.M. (1998). The yeast Saccharomyces cerevisiae contains two glutaredoxin genes that are required for protection against reactive oxygen species. Mol. Biol. Cell *9*, 1081–1091.

Luong, P., Kinch, L.N., Brautigam, C.A., Grishin, N.V., Tomchick, D.R., and Orth, K. (2010). Kinetic and structural insights into the mechanism of AMPylation by VopS Fic domain. J. Biol. Chem. *285*, 20155–20163.

Madej, T., Lanczycki, C.J., Zhang, D., Thiessen, P.A., Geer, R.C., Marchler-Bauer, A., and Bryant, S.H. (2014). MMDB and VAST+: tracking structural similarities between macromolecular complexes. Nucleic Acids Res. *42*, D297–D303.

Manning, G., Whyte, D.B., Martinez, R., Hunter, T., and Sudarsanam, S. (2002). The protein kinase complement of the human genome. Science *298*, 1912–1934.

McLain, A.L., Szweda, P.A., and Szweda, L.I. (2011). α-Ketoglutarate dehydrogenase: a mitochondrial redox sensor. Free Radic. Res. *45*, 29–36.

Mieyal, J.J., and Chock, P.B. (2012). Posttranslational modification of cysteine in redox signaling and oxidative stress: Focus on s-glutathionylation. Antioxid. Redox Signal. *16*, 471–475.

Min, X., Lee, B.H., Cobb, M.H., and Goldsmith, E.J. (2004). Crystal structure of the kinase domain of WNK1, a kinase that causes a hereditary form of hypertension. Structure *12*, 1303–1311.

Minor, W., Cymborowski, M., Otwinowski, Z., and Chruszcz, M. (2006). HKL-3000: the integration of data reduction and structure solution–from diffraction images to an initial model in minutes. Acta Crystallogr. D Biol. Crystallogr. *62*, 859–866.

Müller, M.P., Peters, H., Blümer, J., Blankenfeldt, W., Goody, R.S., and Itzen, A. (2010). The Legionella effector protein DrrA AMPylates the membrane traffic regulator Rab1b. Science *329*, 946–949.

Neal, S.E., Dabir, D.V., Tienson, H.L., Horn, D.M., Glaeser, K., Ogozalek Loo, R.R., Barrientos, A., and Koehler, C.M. (2015). Mia40 Protein Serves as an Electron Sink in the Mia40-Erv1 Import Pathway. J. Biol. Chem. *290*, 20804–20814.

Nguyen, K.B., Sreelatha, A., Durrant, E.S., Lopez-Garrido, J., Muszewska, A., Dudkiewicz, M., Grynberg, M., Yee, S., Pogliano, K., Tomchick, D.R., et al. (2016). Phosphorylation of spore coat proteins by a family of atypical protein kinases. Proc. Natl. Acad. Sci. USA *113*, E3482–E3491.

Otwinowski, Z., Borek, D., Majewski, W., and Minor, W. (2003). Multiparametric scaling of diffraction intensities. Acta Crystallogr. A *59*, 228–234.

Rak, M., Tetaud, E., Godard, F., Sagot, I., Salin, B., Duvezin-Caubet, S., Slonimski, P.P., Rytka, J., and di Rago, J.P. (2007). Yeast cells lacking the mitochondrial gene encoding the ATP synthase subunit 6 exhibit a selective loss of complex IV and unusual mitochondrial morphology. J. Biol. Chem. *282*, 10853–10864.

Roux, K.J., Kim, D.I., and Burke, B. (2013). BioID: a screen for protein-protein interactions. Curr Protoc Protein Sci. *74*. https://doi.org/10.1002/0471140864.ps1923s74.

Saaranen, M.J., Salo, K.E., Latva-Ranta, M.K., Kinnula, V.L., and Ruddock, L.W. (2009). The C-terminal active site cysteine of Escherichia coli glutaredoxin 1 determines the glutathione specificity of the second step of peptide deglutathionylation. Antioxid. Redox Signal. *11*, 1819–1828.

Salomon, D., Guo, Y., Kinch, L.N., Grishin, N.V., Gardner, K.H., and Orth, K. (2013). Effectors of animal and plant pathogens use a common domain to bind host phosphoinositides. Nat. Commun. *4*, 2973.

Salomon, D., and Sessa, G. (2010). Identification of growth inhibition phenotypes induced by expression of bacterial type III effectors in yeast. J. Vis. Exp. *30*, 1865.

Schrodinger, LLC (2015). The PyMOL Molecular Graphics System, Version 1.8.

Shapiro, B.M., and Stadtman, E.R. (1968). 5'-adenylyl-O-tyrosine. The novel phosphodiester residue of adenylylated glutamine synthetase from *Escherichia coli*. J Biol Chem. *243*, 3769–3771.

Shelton, M.D., Chock, P.B., and Mieyal, J.J. (2005). Glutaredoxin: role in reversible protein s-glutathionylation and regulation of redox signal transduction and protein translocation. Antioxid. Redox Signal. *7*, 348–366.

Shi, F., Telesco, S.E., Liu, Y., Radhakrishnan, R., and Lemmon, M.A. (2010). ErbB3/HER3 intracellular domain is competent to bind ATP and catalyze autophosphorylation. Proc. Natl. Acad. Sci. USA *107*, 7692–7697.

Stadtman, T.C. (1974). Selenium biochemistry. Science *183*, 915–922.

Sun, R., Eriksson, S., and Wang, L. (2012). Oxidative stress induced S-glutathionylation and proteolytic degradation of mitochondrial thymidine kinase 2. J. Biol. Chem. *287*, 24304–24312.

Tagliabracci, V.S., Engel, J.L., Wen, J., Wiley, S.E., Worby, C.A., Kinch, L.N., Xiao, J., Grishin, N.V., and Dixon, J.E. (2012). Secreted kinase phosphorylates extracellular proteins that regulate biomineralization. Science *336*, 1150–1153.

Tagliabracci, V.S., Wiley, S.E., Guo, X., Kinch, L.N., Durrant, E., Wen, J., Xiao, J., Cui, J., Nguyen, K.B., Engel, J.L., et al. (2015). A Single Kinase Generates the Majority of the Secreted Phosphoproteome. Cell *161*, 1619–1632.

Takeda, K., Cabrera, M., Rohde, J., Bausch, D., Jensen, O.N., and Ungermann, C. (2008). The vacuolar V1/V0-ATPase is involved in the release of the HOPS subunit Vps41 from vacuoles, vacuole fragmentation and fusion. FEBS Lett. *582*, 1558–1563.

Taylor, S.S., and Kornev, A.P. (2011). Protein kinases: evolution of dynamic regulatory proteins. Trends Biochem. Sci. *36*, 65–77.

Taylor, S.S., Shaw, A., Hu, J., Meharena, H.S., and Kornev, A. (2013). Pseudokinases from a structural perspective. Biochem. Soc. Trans. *41*, 981–986.

Tu, B.P., Kudlicki, A., Rowicka, M., and McKnight, S.L. (2005). Logic of the yeast metabolic cycle: temporal compartmentalization of cellular processes. Science *310*, 1152–1158.

Wagner, T., Bellinzoni, M., Wehenkel, A., O'Hare, H.M., and Alzari, P.M. (2011). Functional plasticity and allosteric regulation of α-ketoglutarate decarboxylase in central mycobacterial metabolism. Chem. Biol. *18*, 1011–1020.

Wollweber, L. (1990). E. Harlow and D. Lane (Editors), Antibodies: A Laboratory Manual. XIII + 726 S., 50 Abb., 62 Tab. Cold Spring Harbor 1988. Cold Spring Harbor Laboratory. $50.00. ISBN: 0-87969-314-2. J Basic Microbiology *30*, 164.

Worby, C.A., Mattoo, S., Kruger, R.P., Corbeil, L.B., Koller, A., Mendez, J.C., Zekarias, B., Lazar, C., and Dixon, J.E. (2009). The fic domain: regulation of cell signaling by adenylylation. Mol Cell. *34*, 93–103.

Xiao, J., Worby, C.A., Mattoo, S., Sankaran, B., and Dixon, J.E. (2010). Structural basis of Fic-mediated adenylylation. Nat. Struct. Mol. Biol. *17*, 1004–1010.

Yarbrough, M.L., Li, Y., Kinch, L.N., Grishin, N.V., Ball, H.L., and Orth, K. (2009). AMPylation of Rho GTPases by Vibrio VopS disrupts effector binding and downstream signaling. Science *323*, 269–272.

Zadziński, R., Fortuniak, A., Biliński, T., Grey, M., and Bartosz, G. (1998). Menadione toxicity in Saccharomyces cerevisiae cells: activation by conjugation with glutathione. Biochem. Mol. Biol. Int. *44*, 747–759.

Zeqiraj, E., and van Aalten, D.M. (2010). Pseudokinases-remnants of evolution or key allosteric regulators? Curr. Opin. Struct. Biol. *20*, 772–781.

Zhu, Q., Venzke, D., Walimbe, A.S., Anderson, M.E., Fu, Q., Kinch, L.N., Wang, W., Chen, X., Grishin, N.V., Huang, N., et al. (2016). Structure of protein O-mannose kinase reveals a unique active site architecture. eLife *5*, e22238.

STAR★METHODS

KEY RESOURCES TABLE

REAGENT or RESOURCE	SOURCE	IDENTIFIER
Antibodies		
Rabbit anti-ScSelO	This study	N/A
Rabbit anti-Thr AMP	(Hao et al., 2011)	N/A
Rabbit anti-Mia40	(Neal et al., 2015)	N/A
High sensitivity streptavidin HRP	Pierce	Cat#21130
Rabbit anti-GroEL	Enzo life sciences	Cat#ADI-SPS-875-D
Mouse anti-GAPDH	ThermoFisher	Cat#MA5-15738
Mouse anti-porin	Invitrogen	Cat#459500
Mouse anti-GSH	ThermoFisher (Virogen)	Cat#NC0324350
Rabbit anti-Vma6	(Takeda et al., 2008)	N/A
Rabbit anti-histone H3	Millipore	Cat#06-755
Donkey anti Mouse IgG, HRP-Linked Whole Ab	VWR	Cat#95017-554
Donkey anti Rabbit IgG, HRP-Linked Whole Ab	VWR	Cat# 95017-556
Bacterial Strains		
Rosetta DE3	Novagen	Cat#70954
Rosetta DE3 ΔSelO (F^- *ompT hsdSB*(rB- mB-) *gal dcm* (DE3) pRARE (CamR) ydiU::Tet)	This study	N/A
Chemicals, Peptides, and Recombinant Proteins		
P. syringae SelO recombinant protein	This study	N/A
E. coli SelO (ydiU) recombinant protein	This study	N/A
S. cerevisiae SelO (FMP40) recombinant protein	This study	N/A
Human SelO (U667C) recombinant protein	This study	N/A
E. coli sucA recombinant protein	This study	N/A
E. coli grxA recombinant protein	This study	N/A
E. coli trxA	This study	N/A
E. coli trxB	This study	N/A
PfuTurbo DNA Polymerase	Thermo	Cat#50-125-946
Myelin basic protein	Sigma	Cat# M1891
Adenosine 5′-triphosphate disodium salt hydrate	Sigma	Cat# A2383
Guanosine 5′-triphosphate sodium salt hydrate	Sigma	Cat# G8877
Cytidine 5′-triphosphate disodium salt	Sigma	Cat# C1506
Uridine 5′-triphosphate trisodium salt hydrate	Sigma	Cat# U6625
Adenosine 5′-(β,γ-imido)triphosphate lithium salt hydrate	Sigma	Cat# A2647
Biotin-17-adenosine-5′-triphosphate	Enzo Life Sciences	Cat# ENZ-42817
ATP, [α-32P]- 3000Ci/mmol 10mCi/ml, 250 μCi	PerkinElmer	BLU003H250UC
ATP, [γ-32P]- 6000Ci/mmol 10mCi/mL, 1mCi	PerkinElmer	BLU002Z001MC
Tris-(2-Carboxyethyl)phosphine, Hydrochloride (TCEP)	Fisher Scientific	Cat# PI20490
Menadione	Sigma	Cat# M5625
Hydrogen peroxide	Sigma	Cat# H1009
4-Acetamido-4'-Maleimidylstilbene-2, 2′-Disulfonic Acid, Disodium Salt	Thermo Fisher Scientific	Cat# A485
β-Nicotinamide adenine dinucleotide 2′-phosphate reduced tetrasodium salt hydrate	Sigma	Cat# N1630

(*Continued on next page*)

Continued

REAGENT or RESOURCE	SOURCE	IDENTIFIER
Oxidized L-glutathione	Sigma	Cat# G4376
Diamide	Sigma	Cat# D3648
High capacity streptavidin agarose resin	Pierce	Cat# 20357
Hygromycin B	Sigma	H7772
Tetracycline	Sigma	87128
Deposited Data		
P. syringae SelO structure	This study	PDB: 6EAC
Experimental Models: Organisms/Strains		
BY4741 (*Mata leu2Δ0 met15Δ0 ura3Δ0 his3Δ1)*	Dharmacon	Cat# YSC1053
BY4741pRS313 (*Mata leu2Δ0 met15Δ0 ura3Δ0 his3Δ1* (pRS313- HIS3/CEN-ARS/Amp)	This study	N/A
BY4741 ΔSelO (*Mata leu2Δ0 met15Δ0 ura3Δ0 his3Δ1 fmp40Δ::KanMX)*	Dharmacon	Cat# YSC1053
BY4741 ΔSelO pRS313 (*Mata leu2Δ0 met15Δ0 ura3Δ0 his3Δ1 fmp40Δ::KanMX* (pRS313- HIS3/ CEN-ARS/Amp))	This study	N/A
BY4741 ΔSelO pRS313 SelO (*Mata leu2Δ0 met15Δ0 ura3Δ0 his3Δ1 fmp40Δ::KanMX* (pRS313- WT FMP40/HIS3/CEN-ARS/Amp))	This study	N/A
BY4741 ΔSelO pRS313 D348A SelO (*Mata leu2Δ0 met15Δ0 ura3Δ0 his3Δ1 fmp40Δ::KanMX* (pRS313- D348A FMP40/HIS3/CEN-ARS/Amp))	This study	N/A
BY4741 cit1 mCherry pDGFP SelO *(Mata leu2Δ0 met15Δ0 ura3Δ0 his3Δ1 cit1-mCherry-HygMX* (pDGFP-P_{GAL1}-*FMP40-GFP/CEN-ARS/Amp)*	This study	N/A
BY4741 cit1 mCherry pDGFP SelO 24-C (*Mata leu2Δ0 met15Δ0 ura3Δ0 his3Δ1 cit1-mCherry-HygMX* (pDGFP-P_{GAL1}-*FMP40 24-C-GFP/CEN-ARS/Amp))*	This study	N/A
MR6 (*Mata ade2-1 his3-11,15 trp1-1 leu2-3,112 ura3-1 CAN1 arg8::hisG)*	1. (Rak et al., 2007)	N/A
MR6 pRS315 (*Mata ade2-1 his3-11,15 trp1-1 leu2-3,112 ura3-1 CAN1 arg8::hisG* (pRS315-LEU2/CEN-ARS/Amp))	This study	N/A
MR6 ΔSelO (*Mata ade2-1 his3-11,15 trp1-1 leu2-3,112 ura3-1 CAN1 arg8::hisG fmp40Δ::KanMX)*	This study	N/A
MR6 ΔSelO pRS315 (*Mata ade2-1 his3-11,15 trp1-1 leu2-3,112 ura3-1 CAN1 arg8::hisG fmp40Δ::KanMX* (pRS315-LEU2/CEN-ARS/Amp))	This study	N/A
MR6 ΔSelO pRS315-WT FMP40 (*Mata ade2-1 his3-11,15 trp1-1 leu2-3,112 ura3-1 CAN1 arg8::hisG fmp40Δ::KanMX* (pRS315- WT FMP40/LEU2/CEN-ARS/Amp))	This study	N/A
MR6 ΔSelO pRS315-D348A FMP40 (*Mata ade2-1 his3-11,15 trp1-1 leu2-3,112 ura3-1 CAN1 arg8::hisG fmp40Δ::KanMX* (pRS315- D348A FMP40/LEU2/CEN-ARS/Amp))	This study	N/A
Oligonucleotides		
See Table S3 for primers used in this study	N/A	N/A
Recombinant DNA		
ppSumo-*E. coli* SelO	This study	N/A
ppSumo-*S. cerevisiae* SelO	This study	N/A

(*Continued on next page*)

Continued		
REAGENT or RESOURCE	SOURCE	IDENTIFIER
ppSumo-*H. sapiens* SelO	This study	N/A
ppSumo-*P. syringae* SelO	This study	N/A
pDGFP-*S. cerevisiae* SelO	This study	N/A
pDGFP-*S. cerevisiae* SelO 24-C	This study	N/A
petDuet1-sucA:SelO	This study	N/A
petDuet1-grxA:SelO	This study	N/A
pProEX-grxA	This study	N/A
pRS313-*fmp40*gene	This study	N/A
pRS315-*fmp40*gene	This study	N/A
pBAD-*Myc*-His	Invitrogen	Cat# V440-01
ppSumo	(Nguyen et al., 2016)	N/A
pDGFP	(Salomon et al., 2013)	N/A
Petduet1	Novagen	Cat# 71146
Software and Algorithms		
Pymol software	Schrödinger	N/A
WebLogo server	(Crooks et al., 2004)	http://weblogo.threeplusone.com/
Dalilite server	(Holm and Rosenström, 2010)	http://ekhidna2.biocenter.helsinki.fi/dali/
Jackhmmer server	(Finn et al., 2015)	https://www.ebi.ac.uk/Tools/hmmer/search/jackhmmer
BLAST server	(Altschul et al., 1990)	https://blast.ncbi.nlm.nih.gov/Blast.cgi
MAFFT server	(Katoh and Standley, 2013)	https://mafft.cbrc.jp/alignment/software/
Pfam database	(Finn et al., 2016)	http://pfam.xfam.org/
Kinase database at kinase.com	(Manning et al., 2002)	www.kinase.com
Reference Proteomes database	(Chen et al., 2011)	https://pir.georgetown.edu/rps/
VAST	(Madej et al., 2014)	https://www.ncbi.nlm.nih.gov/Structure/VAST/vastsearch.html
Phenix	(Adams et al., 2010)	https://www.phenix-online.org
Coot	(Emsley et al., 2010)	https://www2.mrc-lmb.cam.ac.uk/Personal/pemsley/coot/
HKL3000	(Minor et al., 2006)	http://www.hkl-xray.com
GraphPad Prism	N/A	https://www.graphpad.com/scientific-software/prism/

CONTACT FOR REAGENT AND RESOURCE SHARING

Further information and requests for resources and reagents should be directed to and will be fulfilled by the Lead Contact, Vincent S. Tagliabracci (vincent.tagliabracci@utsouthwestern.edu).

EXPERIMENTAL MODEL AND SUBJECT DETAILS

DH5α chemically competent cells were used for molecular cloning. Rosetta (DE3) chemically competent cells were used for protein expression and glutathionylation assays. Both of them were grown in LB medium cultured at 37°C. After induction, Rosetta (DE3) cells were transferred to room temperature. *S. cerevisiae* (BY4741 and MR6) were grown in YPD or YPAD.

The following strains used in this study:

Parental BY4741[*Mata leu2Δ0 met15Δ0 ura3Δ0 his3Δ1*] strain was obtained from Dharmacon and used to generate the following strains: BY4741pRS313 [*Mata leu2Δ0 met15Δ0 ura3Δ0 his3Δ2* (pRS313- HIS3/CEN-ARS/Amp)], BY4741 ΔSelO[*Mata leu2Δ0 met15Δ0 ura3Δ0 his3Δ1 fmp40Δ::KanMX*], BY4741 ΔSelO pRS313 [*Mata leu2Δ0 met15Δ0 ura3Δ0 his3Δ1 fmp40Δ::KanMX* (pRS313- HIS3/CEN-ARS/Amp)], BY4741 ΔSelO pRS313 SelO [*Mata leu2Δ0 met15Δ0 ura3Δ0 his3Δ1 fmp40Δ::KanMX* (pRS313-WT FMP40/HIS3/CEN-ARS/Amp)], BY4741 ΔSelO pRS313 D348A SelO[*Mata leu2Δ0 met15Δ0 ura3Δ0 his3Δ1 fmp40Δ::KanMX* (pRS313- D348A FMP40/HIS3/CEN-ARS/Amp)], BY4741 cit1 mCherry pDGFP SelO[*Mata leu2Δ0 met15Δ0 ura3Δ0 his3Δ1*

cit1-mCherry-HygMX (pDGFP-P_{GAL1}-*FMP40-GFP/CEN-ARS/Amp)*], BY4741 cit1 mCherry pDGFP SelO 24-C[*Mata leu2Δ0 met15Δ0 ura3Δ0 his3Δ1 cit1-mCherry-HygMX* (pDGFP-P_{GAL1}-*FMP40 24-C-GFP/CEN-ARS/Amp)*].

Parental MR6 [*Mata ade2-1 his3-11,15 trp1-1 leu2-3,112 ura3-1 CAN1 arg8::hisG*] strain was obtained from Dr. Jean-Paul di Rago and used to generate the following strains: MR6 pRS315[*Mata ade2-1 his3-11,15 trp1-1 leu2-3,112 ura3-1 CAN1 arg8::hisG* (pRS315-LEU2/CEN-ARS/Amp)], MR6 ΔSelO[*Mata ade2-1 his3-11,15 trp1-1 leu2-3,112 ura3-1 CAN1 arg8::hisG fmp40Δ::KanMX*], MR6 ΔSelO pRS315[*Mata ade2-1 his3-11,15 trp1-1 leu2-3,112 ura3-1 CAN1 arg8::hisG fmp40Δ::KanMX* (pRS315-LEU2/CEN-ARS/Amp)], MR6 ΔSelO pRS315-WT FMP40[*Mata ade2-1 his3-11,15 trp1-1 leu2-3,112 ura3-1 CAN1 arg8::hisG fmp40Δ::KanMX* (pRS315- WT FMP40/LEU2/CEN-ARS/Amp)], MR6 ΔSelO pRS315-D348A FMP40[*Mata ade2-1 his3-11,15 trp1-1 leu2-3,112 ura3-1 CAN1 arg8::hisG fmp40Δ::KanMX* (pRS315- D348A FMP40/LEU2/CEN-ARS/Amp)].

All yeast strains were grown at 30°C in the appropriate experimental growth medium as described in the methods section.

METHOD DETAILS

Reagents

Myelin basic protein (M1891-5MG), Menadione (M5625) and AMP-PNP (A2647) were purchased from Sigma. Selenomethionine containing medium was purchased from Molecular Dimensions (MD12-500). Tris(2-carboxyethyl)phosphine hydrochloride (TCEP; 20490) and 4-acetamido-4'-maleimidylstilbene-2,2′- disulfonic acid (AMS; A485) were purchased from Thermo Fisher. Biotin-17-ATP was purchased from Enzo life sciences (ENZ-42817). High sensitivity streptavidin HRP (21130) and high capacity streptavidin agarose resin (20357) were purchased from Pierce. Rabbit anti-GroEL antibodies were purchased from Enzo life sciences (ADI-SPS-875-D). Rabbit anti-Vma6 antibodies were a generous gift from Dr. Vincent Starai (University of Georgia, Athens). Mouse anti-porin antibodies were from Invitrogen (459500), and rabbit anti-histone H3 antibodies were from Millipore (06-755). Rabbit anti-Mia40 antibodies were a generous gift from Dr. Carla Koehler (UCLA). Rabbit anti AMP-Threonine antibodies were as described previously (Hao et al., 2011). Mouse anti-GSH and anti-GAPDH antibodies were from Thermo.

Generation of constructs and strains

The *E. coli* SelO (ydiU), grxA, sucA, trxA and trxB coding sequence were amplified by PCR using Rosetta genomic DNA as a template. The *Pseudomonas syringae* SelO coding sequence was amplified by PCR using *P. syringae* DC3000 genomic DNA. The *S. cerevisiae* coding sequence was amplified using BY4741 genomic DNA as a template. *Homo sapiens* SelO cDNA clone was a generous gift from Carolyn Worby (UCSD). The amplified open reading frames were cloned into a modified pet28a bacterial expression vector (ppSumo), containing an N-terminal 6X-His tag followed by the yeast Sumo (smt3) coding sequence or pProEX2 containing an N-terminal 6X-His tag followed by a TEV protease cleavage site.

BY4741 cit1-mCherry was derived from BY4741 (*MATa his3Δ1 leu2Δ0 met15Δ0 ura3Δ0*) using a PCR-based modification (Longtine et al., 1998). Briefly, a mCherry and hygromycin resistance cassette with homologous sequences flanking the C terminus of the Cit1 gene was amplified by PCR. The product of the reaction was then introduced to BY4741 via a lithium acetate mediated transformation and recovered overnight in 2 mL of YPD. Recombinants were selected by plating 100 μL of the transformation on YPD agarose plates supplemented with 200 μg/mL hygromycin. Successful recombination was verified by colony PCR using primers flanking the endogenous locus and the inserted cassette.

The *S. cerevisiae* SelO (*fmp40)* gene was replaced by *KANMX4* deletion cassette in the W303-1B strain background (MR6, *MATa ade2-1 his3-11,15 trp1-1 leu2-3,112 ura3-1 CAN1 arg8::hisG*) (Rak et al., 2007). The cassette was amplified by PCR with primers FWD:5′-CGGTGATATGAGGTGATCGTGG-3′ and REV:5′-GGTGCCAGTCGTTCGG-3′, using total gDNA isolated from *fmp40::KANMX4* deletion mutant as a template (Euroscarf collection). After transformation and selection on plates supplemented with geneticin at 200 μg/mL. Deletions were verified by PCR using primers 5′-GAACTCCGGAATTGGACGATG-3′ and internal primer to the KANMX4 gene 5′-GGATGTATGGGCTAAATGTACG-3′.

For yeast complementation experiments, the *S. cerevisiae* SelO gene containing 1000 bp upstream of the ATG and 500 bp of the 3′UTR was cloned into the pRS313 vector using Not1 and Spe1 endonucleases. The FMP40 gene was then subcloned into the pRS315 vector using Not1 and Sma1, which deleted ~130 bp from the 3′UTR.

The *E. coli* SelO (ydiU) gene was disrupted using the λ red recombinase-mediated recombination system (Datsenko and Wanner, 2000). Briefly, a tetracycline resistance cassette flanked with 50 bp homologous to the ydiU gene was amplified via PCR. The reaction product was electroporated into the Rosetta *E. coli* strain carrying the λ red recombinase plasmid pKD46 (a generous gift from the Dr. Vanessa Sperandio). Transformants were selected by growth on LB agar plates containing tetracycline (10 μg/mL) and simultaneously cured of pKD46 by growth at 37°C overnight. Disruption of the *ydiU* gene was confirmed by colony PCR, using primers flanking the endogenous locus and the inserted cassette.

Protein purification

E. coli, P. syringae, S. cerevisiae or *H. sapiens* SelO, cloned into ppSumo, were transformed into Rosetta DE3 cells. Cells were grown in Luria Bertani (LB) broth to OD_{600} of 0.6-0.8. Protein expression was induced with 0.4 mM IPTG for 16-18 hours at room temperature. Cells were harvested by centrifugation and lysed in 50mM Tris-HCl pH 8, 300 mM NaCl, 1 mM PMSF by sonication. Cell lysates were cleared by centrifugation at 25,000 −30,000 x g for 25-30 min. The cleared lysate was incubated with washed

Ni-NTA beads for one hour at 4°C. Beads were passed over a column and washed with 20 column volumes of 50 mM Tris-HCl pH 8, 300 mM NaCl, 10-25 mM imidazole. Fusion proteins were eluted with 50mM Tris-HCl pH 8, 300 mM NaCl, 300 mM imidazole. Proteins were cut overnight at 4°C with 6X-His tagged ULP Sumo protease followed by gel filtration chromatography using a Superdex 200 gel filtration column attached to an AKTA Pure FPLC chromatography system (GE Healthcare). When proteins were purified in the presence of reducing agent, 0.1% β-mercaptoethanol was added to the lysis buffer. The wash, elution and gel filtration buffers contained 1 mM DTT.

In vitro AMPylation assays

For comparison of [γ-^{32}P]ATP with [α-^{32}P]ATP, assays were performed using purified, untagged *E. coli, S. cerevisiae* or *H. sapiens* SelO in a reaction mixture containing 50 mM Tris-HCl pH 8, 5 mM $MgCl_2$, 100 μM [γ-^{32}P]ATP or [α-^{32}P]ATP (specific radioactivity = 3000 cpm/pmol), 5 mM DTT, and 100 μg/mL SelO proteins. Reactions were incubated at 37°C for 30 min and terminated by adding 25 mM EDTA. SDS loading buffer was then added to the samples and boiled. Reaction products were resolved by SDS-PAGE and stained with Coomassie blue.

Typically, AMPylation assays were performed in a reaction mixture containing 50 mM Tris-HCl pH 8, 5 mM $MgCl_2$, 100 μM [α-^{32}P] ATP (SA = 500-3000 cpm/pmol), 10-50 μg/mL SelO, and 250 μg/mL of substrate (myelin basic protein or grxA). Reactions were also performed with 5 mM DTT, 0.1 mM to 2 mM excess GTP, CTP or UTP nucleotide, or with the thioredoxin system (13 μM *E. coli* trxA, 5 μM *E. coli* trxB and 200 μM NADPH). Reactions were incubated at 37°C for various time points and terminated by adding EDTA. SDS loading buffer containing 1% β-mercaptoethanol was added to samples and boiled. Samples were resolved by SDS-PAGE and stained with Coomassie blue.

For SelO point mutant AMPylation reactions (Figure 4B), assays were performed using Sumo tagged *E. coli* SelO, under the same conditions as above for 15 min using 250 μg/mL MBP as substrate. Reactions were terminated by adding EDTA and SDS loading buffer with 1% β-mercaptoethanol and boiled. Reaction products were resolved by SDS-PAGE and stained with Coomassie blue. MBP bands were excised and the incorporated radioactivity was quantified by scintillation counting using a Beckman scintillation counter.

For non-radioactive auto AMPylation reactions, untagged *E. coli or* human SelO was incubated in 50 mM Tris-HCl pH 8, 5 mM $MgCl_2$, 100 μM ATP, 5 mM DTT for 1 hour at 37°C. Reactions were terminated by adding EDTA and SDS loading buffer with 1% β-mercaptoethanol and boiled. Reaction products were resolved by SDS-PAGE, transferred to a nitrocellulose membrane and immunoblotted with rabbit anti-Thr AMP antibody. Immunoblotting was essentially performed as described (Tagliabracci et al., 2015). Briefly, membranes were blocked with 5% BSA for 1 hour at room temperature. The membranes were briefy rinsed with filtered 50 mM Tris-HCl pH 7.5, 150 mM NaCl, 0.1% tween 20 (TBST). Membranes were incubated with anti-Thr AMP antibody (1:1000) diluted in 2% nonfat dry milk (Kroger) overnight at 4°C with shaking. The membranes were washed 3-4X for 10 min each with TBST at room temperature. The membranes were then probed with donkey anti-rabbit IgG, HRP linked (1:5000 in 2% milk) for 1 hour at room temperature followed by 3-4 washes with TBST and detection by chemiluminescence.

SelO reduction assay

For redox assays, 100 μg/mL (1.8 μM) untagged *E. coli* SelO was incubated with 0, 0.03, 0.1, 0.3 or 1 mM DTT in 50 mM Tris-HCl pH 7.5, 150 mM NaCl for 1 hour at room temperature. SDS loading buffer without reducing agent was added to samples and boiled. Samples were resolved by SDS-PAGE and stained with Coomassie blue.

Production of *S. cerevisiae* SelO antibodies

S. cerevisiae SelO was purified as a 6X His-Sumo fusion protein as above and the His-Sumo tag was cleaved with ULP1. The untagged protein was purified by Superdex 200 gel filtration chromatography and used to inoculate rabbits for generation of rabbit anti-*S. cerevisiae* SelO anti-serum (Cocalico Biologicals). Total IgG was partially purified by ammonium sulfate precipitation (Kent, 1999) then passed over a HiTrap NHS-activated HP column (GE Healthcare) linked to 6X His-Sumo to remove any potential contaminating anti-Sumo IgG. Anti-*S. cerevisiae* SelO antibodies were affinity-purified from the flow through by coupling *S. cerevisiae* SelO to a new HiTrap NHS-activated HP column essentially as described (Wollweber, 1990).

S. cerevisiae confocal microscopy

The *S. cerevisiae* SelO (*fmp40*) was cloned into a modified yeast expression vector containing a C-terminal GFP-myc tag (pDGFP) (Salomon et al., 2013). The BY4741 cit1 mCherry strain was transformed with empty vector, pDGFP, pDGFP *S. cerevisiae* SelO or pDGFP *S. cerevisiae* SelO 24-C. Transformed cells were grown overnight in synthetic drop-out (SD) medium without uracil and containing 2% glucose. The following day, cells were harvested by centrifugation and washed three times with sterile water. Cells were placed in culture at 30°C with shaking for 8 hours in SD-medium without uracil and containing 1% Galactose / 2% Raffinose. Cells were spotted on glass coverslip and used for confocal imaging on a Zeiss LSM 800 confocal microscope.

S. cerevisiae mitochondria isolation

Yeast mitochondria were isolated as previously described (Gregg et al., 2009). Briefly, yeast cells were pelleted by centrifugation at 3000 x g for 5 min and the cells were washed with water then resuspended in DTT buffer (100 mM Tris-HCl pH 9.4, 10mM DTT). The

cells were then incubated with shaking at 30°C for 20 min and pelleted by centrifugation. Cells were washed with zymolase buffer (20 mM potassium phosphate pH 7.4, 1.2 M sorbitol) and resuspended in zymolase buffer containing lyticase. Cells were incubated at 30°C for 30 min with shaking, then pelleted by centrifugation at 2200 x g for 5 min at 4°C. The resulting spheroplasts were washed with ice cold homogenization buffer (10 mM Tris-HCl pH 7.4, 0.6 M sorbitol, 1 mM EDTA, 0.2% BSA). Spheroplasts were resuspended in ice cold homogenization buffer and lysed using a glass dounce homogenizer. Spheroplasts were then centrifuged at 1500 x g for 5 min at 4°C and the supernatant was centrifuged at 3000 x g for 5 min at 4°C. The resulting supernatant was further centrifuged at 12,000 x g for 15 min at 4°C. The pellet was resuspended in SEM buffer (10 mM MOPS KOH pH 7.2, 250 mM sucrose, 1 mM EDTA) and centrifuged at 3000 x g for 5 min at 4°C. The supernatant was centrifuged at 12,000 x g for 15 min at 4°C. The pellet, which contains enriched mitochondria, was used for SelO TCA precipitation and glutathionylation assays (see below).

S. cerevisiae sucrose gradient fractionation

BY4741 or BY4741 Δ*SelO* (Dharmacon YSC1053) were grown overnight at 30°C in YPD broth (20 g/L peptone, 10 g/L yeast extract, 2% glucose) and harvested by centrifugation. Yeast cells were disrupted and fractionated as described above. The enriched mitochondrial pellet was applied to a sucrose gradient, which was prepared by overlaying 15% sucrose in EM buffer (10 mM MOPS KOH pH 7.2, 1 mM EDTA) over 30%, 45%, 60% and 75% sucrose. Proteins (2 μg) from each sucrose gradient fraction were resolved by SDS-PAGE, transferred to nitrocellulose and immunoblotted with rabbit anti-*S. cerevisiae* SelO, mouse anti-porin, rabbit anti-Vma6 or rabbit anti-histone H3 antibodies.

SelO TCA precipitation

BY4741 or BY4741 Δ*SelO* grown in YPD broth overnight at 30°C was harvested by centrifugation. Yeast mitochondria were isolated as described above. Mitochondria (100 μg) were pelleted and resuspended in 1 mL of 10% ice cold trichloroacetic acid (TCA). Mitochondrial proteins were precipitated on ice for 1 hour, then centrifuged at 20,000 x g for 10 min at 4°C. Precipitated pellets were washed with 1 mL of ice cold acetone and centrifuged at 20,000 x g for 5 min at 4°C. Pellets were air-dried and resuspended in 200 μL of 500 mM Tris-HCl, pH 7.5, 2% SDS and 1 mM EDTA. Samples were incubated for 10 min at room temperature in the presence or absence of 5 mM DTT. SDS loading buffer without reducing agent was added to the samples, which were subsequently resolved by SDS-PAGE and transferred to nitrocellulose membrane.

SelO cysteine mutant reduction assay

E. coli SelO was purified as described above in the absence of reducing agent. Untagged *E. coli* SelO (100 μg/mL) was incubated in the presence or absence of 1 mM TCEP and/or 5 mM AMS for 2 hours at room temperature in the dark. SDS loading buffer without reducing agent was added to samples. Samples were resolved by SDS-PAGE and stained with Coomassie blue.

Biotin-17-ATP AMPylation assay

Assays were performed using purified untagged *E. coli* SelO in a reaction mixture containing 50 mM Tris-HCl pH 8, 5 mM $MgCl_2$, 5mM DTT, 500 μM biotin-17-ATP, 200 μg/mL SelO, 300 μg/mL *E. coli* cell lysate or yeast mitochondrial extracts. Reactions were also performed after pretreating *E. coli* and yeast mitochondria with either 2 mM H_2O_2 (*E. coli*) or 0.5 mM (yeast mitochondria). Biotinylation reactions were incubated at 37°C for 30 min and terminated by the addition of EDTA and SDS loading buffer with 1% β-mercaptoethanol and boiled. Reaction products were resolved by SDS-PAGE and transferred to nitrocellulose membranes. The Streptavidin HRP blot was performed as previously described (Roux et al., 2013). Briefly, the membranes were incubated in 1X PBS containing 1% BSA and 0.2% Triton X-100 for 30 min at room temperature. The membranes were then incubated with streptavidin-HRP at 1:40,000 dilution in 1X PBS containing 1% BSA and 0.2% Triton X-100 with shaking overnight at 4°C. Membranes were washed and blocked with 1X PBS containing 10% adult bovine serum and 1% Triton X-100 for 5 min at room temperature. Membranes were washed with 1X PBS and blots were developed using enhanced chemiluminescence (ECl) and visualized by chemiluminescence For streptavidin agarose pulldowns, reactions were terminated with EDTA, then affinity purified using streptavidin agarose as previously described (Roux et al., 2013). Briefly, the streptavidin agarose beads containing the biotinylated proteins were washed with 2% SDS for 8 min at room temperature followed by washing with 50 mM HEPES pH 7.5, containing 0.1% deoxycholic acid, 1% Triton X-100, 1 mM EDTA and 500mM NaCl. The beads were then washed again with 10mM Tris-HCl pH 7.4, 0.5% deoxycholic acid, 0.5% NP-40, 1 mM EDTA and 250 mM LiCl followed by a final wash with 50mM Tris-HCl pH 7.4 prior to MS analysis.

In vivo sucA and grxA AMPylation assays

E. coli sucA and grxA were cloned into the MCS1 of petDuet1 in frame with an N-terminal 6X His tag. *E. coli* SelO was cloned without a tag into the MCS2 of petDuet1. SelO D256A, sucA T405A and sucA S404A were generated by site directed mutagenesis as described (Nguyen et al., 2016). Briefly, primers were designed using the Agilent Quick Change Primer design tool: https://www.genomics.agilent.com/primerDesignProgram.jsp and used in PCR reaction to generate the desired mutation using PfuTurbo DNA polymerase (Thermo). Reaction products were digested with Dpn1 restriction endonuclease and mutations were confirmed by sequencing plasmids. petDuet-sucA:SelO or petDuet-grxA:SelO (or mutants) were transformed into Rosetta DE3 Δ *E. coli* SelO (ydiU) strain. Cells were grown in LB broth to OD_{600} = 0.6-0.8. Protein expression was induced by the addition of 0.4 mM IPTG overnight at room

temperature and the His tagged proteins were purified as described above in the presence of reducing agent. His tagged proteins were further purified by Superdex 200 gel filtration column using AKTA Pure FPLC chromatography system. SucA (2 μg) was resolved by SDS-PAGE and immunoblotted with rabbit anti-Thr AMP antibody. sucA and grxA (5 μg) were resolved by SDS-PAGE in preparation for mass spectrometry.

Hydrogen peroxide viability assays

The MR6 strain was transformed with the empty pRS315 vector. The MR6 Δ *S. cerevisiae* SelO strain was transformed with empty vector, WT *S. cerevisiae* pRS315-SelO or pRS315- *S. cerevisiae* SelO D348A. Exponential growth-phase cultures (OD = 1) in glucose minimal medium (0.67% Yeast Nitrogen Base, 2% glucose, leucine Drop-out amino acids, adenine 40 mg/L) were treated with 0.1 mM H_2O_2 for 200 min with shaking at 28°C. The cell survival in the culture at time zero (before the hydrogen peroxide treatment) and after were estimated by plating the cells on the YPD-adenine plates (1% Yeast Extract, 1% bacto peptone, 2% glucose, 2% Bacto agar, adenine 40 mg/L). The % survival was normalized to the number of cells at time zero. Results are representative of three independent experiments.

Menadione viability assays

BY4741 was transformed with empty pRS313 vector. BY4741 Δ *S. cerevisiae* SelO strain was transformed with empty vector, WT *S. cerevisiae* pRS313-SelO or pRS313- *S. cerevisiae* SelO D348A. Exponential growth phase cultures in glucose synthetic drop-out medium without histidine (6.7 g/L yeast nitrogen base without amino acids, 1.4 g/L yeast synthetic drop-out medium supplement and containing 2% [w/v] glucose and leucine, tryptophan, uracil; (Salomon and Sessa, 2010), were treated with 0.6 mM menadione for 1 hour at 30°C. Post treatment, cells were serial diluted ten-fold and spotted on synthetic drop-out plates. Cells were grown for 2-3 days prior to imaging.

Mass spectrometry analysis

Sample preparation included the excision of proteins from polyacrylamide gels that were separated by SDS-PAGE and stained with Coomassie blue. Protein gel samples were reduced and alkylated using DTT and iodoacetamide, respectively. Note, reduction and alkylation of cysteine residues was not performed on the sample containing unreduced *E. coli* SelO peptides linked by the disulfide bond (Figure 5). Enzymatic overnight digestion (37°C) was performed on all samples using trypsin or Asp-N and samples were desalted using solid phase extraction (SPE) prior to mass spectrometry analysis. LC-MS/MS experiments were performed on a Thermo Scientific EASY-nLC 1200 liquid chromatography system coupled to a Thermo Scientific Orbitrap Fusion Lumos mass spectrometer. To generate MS/MS spectra, MS1 spectra were first acquired in the Orbitrap mass analyzer with a resolution of 120,000. Peptide precursor ions were isolated and fragmented using high-energy collision-induced dissociation (HCD). The resulting MS/MS fragmentation spectra were acquired in the ion trap. MS/MS spectral data was then searched using the Mascot search engine (Matrix Science) for peptide identification. Carbamidomethylation of cysteine residues (+57.021 Da) was set as a static modification for searches, while oxidation of methionine (+15.995 Da) and AMPylation of serine/tyrosine/threonine (+329.053 Da) were set as dynamic modifications. The precursor ion tolerance was set to 15 ppm and the product ion tolerance was set to 0.6 Da for all searches. The MS/MS spectrum of the *E. coli* SelO peptides linked by the disulfide bond were first identified using Thermo BioPharma Finder software and confirmed via manual verification and assignment of fragment ions. Carbamidomethylation of cysteine residues was not included as a modification for this search, as the sample was not reduced/alkylated. Additionally, the identification of all AMPylated peptides were manually verified from the MS/MS spectra of the modified peptides and their unmodified counterparts. Unique ions (136.1, 250.1, and 348.1 Da) corresponding to the neutral loss of the AMP group from peptides during HCD were present in the MS/MS spectra of AMPylated peptides.

Analysis of *S. cerevisiae* SelO expression

MR6 and MR6 ΔSelO strain was grown in YPAD overnight, then diluted into YP medium with either 2% glucose, 2% galactose, 2% raffinose, 3% glycerol, 2% potassium acetate, or 2% sodium lactate. Cells were harvested following overnight incubation at 30°C and extracts were prepared as described previously (Salomon and Sessa, 2010). Briefly, 1OD of yeast cells were centrifuged at 800 x g for 5 min at room temperature. Cells were resuspended in 100 uL of ice cold yeast lysis buffer (200 mM NaOH and 0.5% β-mercaptoethanol) and incubated on ice for 30 min. The pH of the lysate was adjusted to ~7 by the addition of 6M HCl. SDS loading buffer containing 1% β-mercaptoethanol was added and the samples were boiled prior to SDS-PAGE.

E. coli protein S-glutathionylation experiments

Rosetta and Rosetta Δ SelO strains were transformed with empty pBad MycHis vector. Cultures were grown in M9 minimal medium with ampicillin for 48 hours. Cells (1 OD) were resupended in 1xPBS and treated with 1 mM GSSG or 1 mM diamide for 25 min at room temperature. Post treatment, 10 mM NEM was added to the cells and incubated for 5 min at room temperature. SDS loading buffer without reducing agent was added to the samples, which were subsequently resolved by SDS-PAGE, transferred to nitrocellulose membranes and analyzed for protein S-glutathionylation using the anti-GSH antibody (Virogen/Thermo) and GroEL.

Yeast protein S-glutathionylation experiments

MR6 and MR6 Δ *S. cerevisiae* SelO strains were grown in YP-glycerol to OD of 0.9. Mitochondria were isolated as described above and treated with 0.5 mM GSSG and/or 0.1 mM diamide for 30 min at room temperature. Post treatment, 10 mM NEM was added to the mitochondria and incubated for 5 min at room temperature. SDS loading buffer without reducing agent was added to the samples, which were subsequently resolved by SDS-PAGE, transferred to nitrocellulose membranes and analyzed for protein S-glutathionylation using the anti-GSH antibody (Virogen/Thermo) and porin.

Crystallization and structure determination

P. syringae SelO at 10 mg/mL in 17 mM Tris-HCl pH 8, 100 mM NaCl, 1 mM TCEP, 5 mM $MgCl_2$, 1 mM AMP-PNP was crystallized at 20°C using the sitting drop vapor-diffusion method with a reservoir solution containing 200 mM calcium acetate, and 22% (w/v) PEG 3350. The crystals were cryo-protected with 200 mM calcium acetate, 22% (w/v) PEG 3350, 100 mM NaCl and 30% ethylene glycol and then flash-cooled in liquid nitrogen. Native crystals diffracted to a minimum Bragg spacing (d_{min}) of 2.27 Å and exhibited the symmetry of space group I222 with cell dimensions of a = 136.2 Å, b = 158.1 Å, c = 227.3 Å and contained four SelO molecules per asymmetric unit. All diffraction data were collected at beamline 19-ID (SBC-CAT) at the Advanced Photon Source (Argonne National Laboratory, Argonne, Illinois, USA) and processed in the program *HKL-3000* (Minor et al., 2006) with applied corrections for effects resulting from absorption in a crystal and for radiation damage (Borek et al., 2003; Otwinowski et al., 2003), the calculation of an optimal error model, and corrections to compensate the phasing signal for a radiation-induced increase of non-isomorphism within the crystal (Borek et al., 2010; Borek et al., 2013). These corrections were crucial for successful phasing. Phases were obtained from a single wavelength anomalous dispersion (SAD) experiment using the selenomethionyl-derivatized SelO protein with data to 2.2 Å. Forty-seven selenium sites were located, phases improved and an initial model containing 98% of all SelO residues was automatically generated in the *AutoBuild* routine of the *Phenix* program suite (Adams et al., 2010). Completion of this model was performed by manual rebuilding in the program *Coot* (Emsley et al., 2010). Positional and isotropic atomic displacement parameter (ADP) as well as TLS ADP refinement was performed to a resolution of 2.27 Å for the Mg^{2+}-Ca^{2+}-AMP-PNP-bound SelO using the program *Phenix* with a random 1.8% of all dataset aside for an R_{free} calculation. The final model for SelO (R_{work} = 18.8%, R_{free} = 21.2%) contained 1,902 residues, four molecules of Mg^{2+}-Ca^{2+}-AMP-PNP, ten additional Ca^{2+} ions, four Cl^- ions, twenty-two ethylene glycol molecules, five polyethylene glycol molecules, four acetates and 590 waters. Residue Asp262 in all four monomers are outliers in a Ramachandran plot as defined in the program *MolProbity* (Chen et al., 2010); the sidechain carboxylate of this residue coordinates the metals of the Mg^{2+}-Ca^{2+}-AMP-PNP. Data collection and structure refinement statistics are summarized in Table S1.

Comparison of SelO active site with Csk1

Structures for canonical kinases (PKs) were selected from a Dalilite (Holm et al., 2008) search against the PDB with hits having DaliZ scores above 8. The structure for IRAK-4 was one of the top-scoring hits: PDB:2nru (DaliZ 9.7) and the structure for Csk1 included a bound ATP: 1csn (DaliZ 8.6). Dalilite alignments against the *P. syringae* structure were used to assemble the multiple sequence alignment of SelO family representatives. The Dalilite structure superposition of Csk1 and *P. syringae* SelO was viewed in Pymol (Schrodinger, 2015) to compare bound nucleotide positions, with the Mg^{2+} and α-, β- and γ -phosphates of AMP-PNP in the SelO structure superimposing with the Mg^{2+} and flipped γ -, β-, and α-phosphates, respectively.

Conservation of human kinases and selenoproteins compared to bacterial homologs

Human protein kinase domain sequences were fetched from www.kinase.com. Domains other than protein kinase-like (PKL) fold were excluded, leaving total of 516 kinase domains. This set was augmented by five human members of the FAM69 family, two members of the FAM198 family, and the SelO protein. Further, this set was augmented by PKL domains from 34 human proteins belonging to the following Pfam (Finn et al., 2016) families: APH, PI3_PI4_kinase, PI3Ka, PIP5K, Fructosamin_kin, IPK, Ins_P5_2-kin, KIND, that were not included in the kinase.com dataset.

The combined dataset included 558 human protein kinase-like (PKL) domains. The protein BLAST program was used to find, for every PKL query, the closest bacterial homolog within the collection of bacterial Reference Proteomes (rp55 list, 2601913 sequences) (Chen et al., 2011). 315 kinases had homologs in bacteria satisfying the requirement of E-value below 0.001.

In a similar fashion, the protein BLAST program was used to find for every of the 25 human selenoproteins its closest bacterial homolog. Out of the 25 selenoproteins, 17 had a bacterial homolog thus defined.

SelO family sequence logo

The sequence of SelO from *Pseudomonas syringae pv. tomato str. DC3000* was subjected to 7 iterations of Jackhmmer search (Finn et al., 2015) against Reference Proteomes in order to build a collection of homologs. The search yielded 3427 aligned protein sequences. The alignment was filtered as to retain only columns present in the *P. syringae* SelO, and used as input to the WebLogo server as shown in Figure S1 (Crooks et al., 2004).

SelO sequences were collected using BLAST (Altschul et al., 1997) (E.value cutoff 0.001) against the filtered RefSeq sequence database with the *P.syringae* sequence (PBQ12144.1) as a query. Sequences were aligned using MAFFT (Katoh and Standley, 2013) to generate conservations and representatives from *E.coli* (NP_416221.1), human (NP_113642.1), yeast (Q08968.1) and plant (NP_196807.2) were selected for the alignment in Figure 1A.

Replication

All experiments were performed 3 times unless otherwise stated.

QUANTIFICATION AND STATISTICAL ANALYSIS

Quantification of yeast cell survival following H_2O_2 treatment is represented as the mean of three independent experiments (n = 3). A Student's t test was used to calculate a p value using GraphPad Prism 7. Error bars represent the standard error of the mean (SEM).

DATA AND SOFTWARE AVAILABILITY

The accession number for the coordinates and structure factors reported in this paper is PDB: 6EAC.

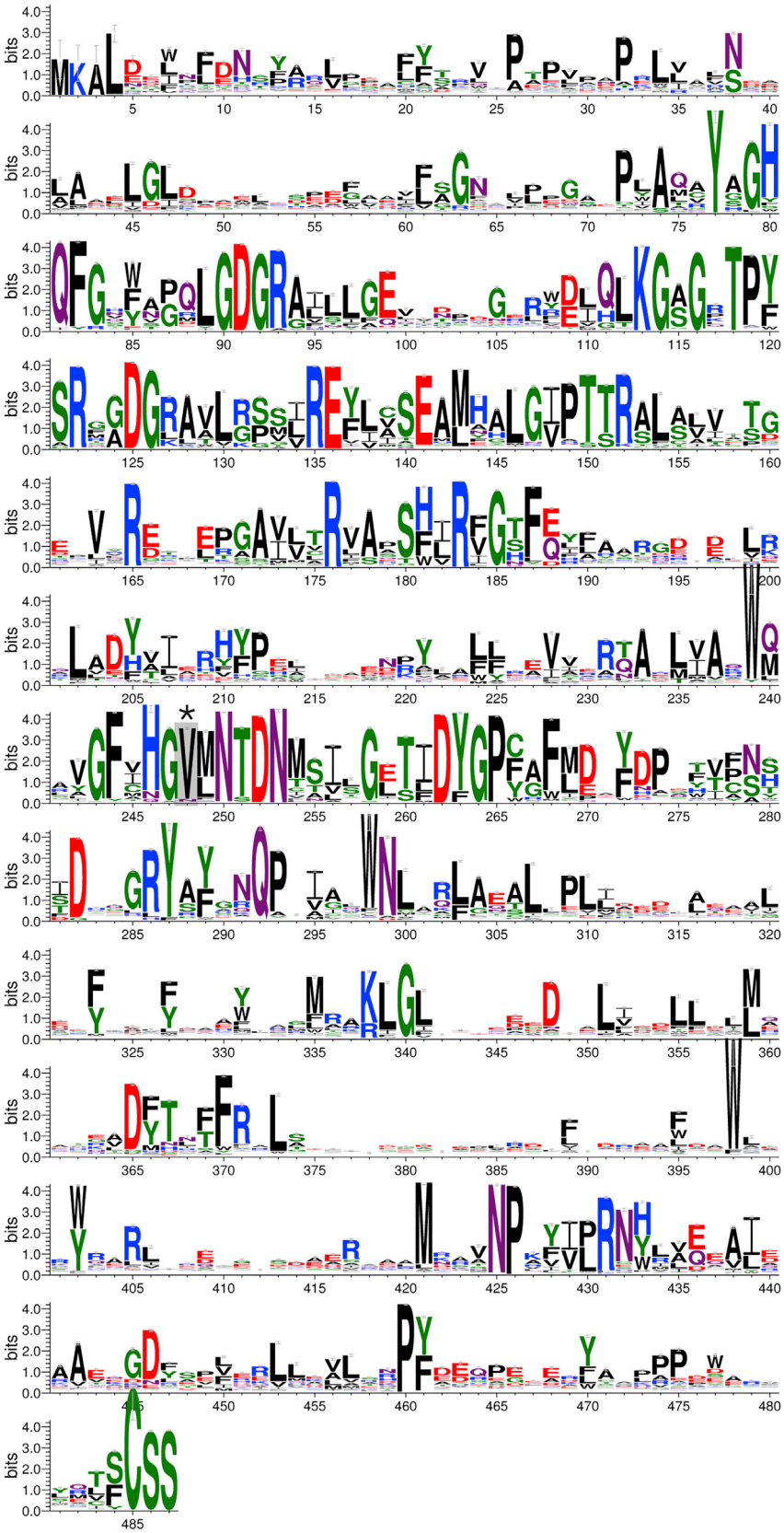

(legend on next page)

Figure S1. SelO Family Sequence Logo, Related to Figure 1

The sequence of *Pseudomonas syringae pv. tomato str. DC3000* SelO was subjected to 7 iterations of Jackhmmer search against Reference Proteomes in order to build a collection of homologs. The search yielded 3427 aligned protein sequences. The alignment was filtered so position numbers match *P. syringae* SelO residues and used as an input to the WebLogo server to generate the figure, which highlights conserved residues in the SelO family of pseudokinases. The height of the amino acid stack indicates the sequence conservation at that position. The position of the missing catalytic Asp (PKA; D166) is shaded and highlighted with an asterisk.

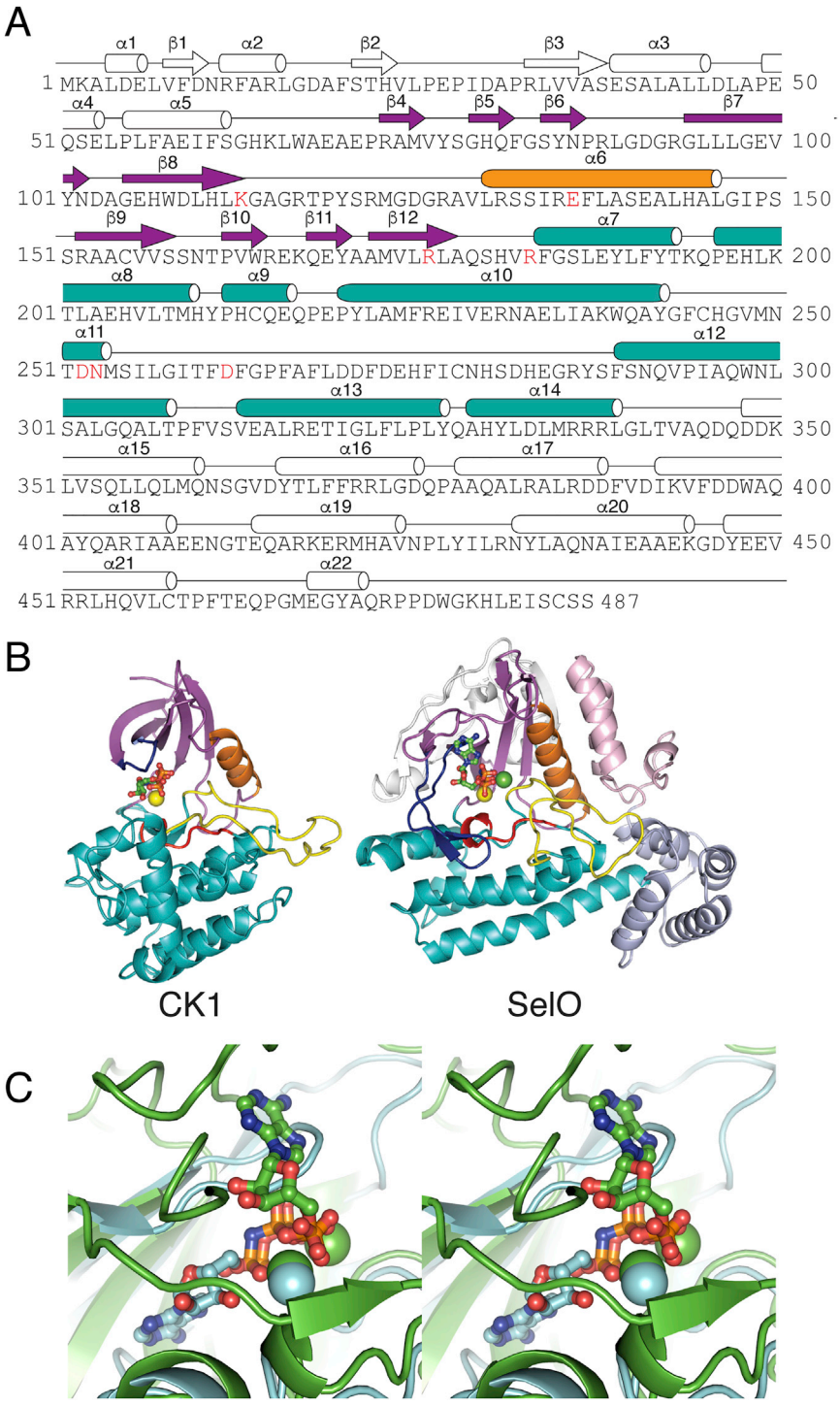

Figure S2. Crystal Structure of *P. syringae* SelO Reveals an Atypical Protein Kinase Fold with a Unique Orientation of the Nucleotide in the Active Site, Related to Figure 2

(A) Amino acid sequence of *P. syringae* SelO depicting the secondary structural elements, color-coded as in Figure 2A.

(B) Ribbon representation of protein kinase CK1 and *P. syringae* SelO. Color coding is shown as in Figure 2A.

(C) Superposition of SelO with CK1 highlights flipped ATP binding mode. Stereo view (crosseye) of SelO pseudokinase (green) bound to AMP-PNP (green ball and stick) superimposed with CK1 (cyan) bound to ATP (cyan ball and stick) reveals flipped nucleotide.

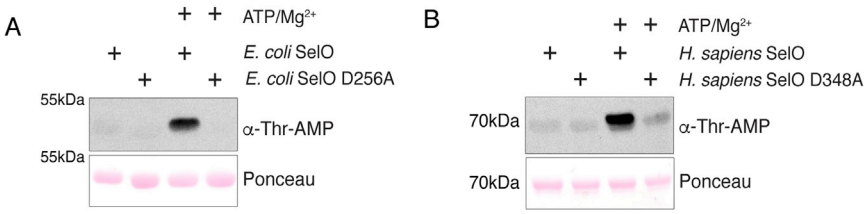

C

Modified Residue	Peptide	Spectral Counts	
		E. coli SelO	*E. coli* SelO D256A
Y114	GAGLTPYSR	4	0
Y158	ALSIVTSDSPVYR	5	0
Y185/Y186	FGHFEHFYYR	1	0
Y281/S282	YSFDNQPAVALWNLQR	2	0
S475/S477/ S478	RLEVSCSS	8	0

Modified Residue	Peptide	Spectral Counts	
		yeast SelO	*yeast* SelO D348A
Y42	KLTADTSLSSIQEAINVVQQYNATDPVR	13	0
Y42	LTADTSLSSIQEAINVVQQYNATDPVR	11	0
Y119	VYYSDSIFPYSTVYSGFQFGSFAAQLGDGR	4	0
Y645	LYLMSVNPYDR	4	0

Modified Residue	Peptide	Spectral Counts	
		Human SelO	*Human* SelO D256A
S24/S26	CSPSPAPR	4	0
T221/S222/ S224/T225	AGACVTSESTVVR	2	0
Y232	DVFYDGNPK	7	0
Y599	NYIAQNAIEAAER	1	0
T625/Y627	LLETPYHCEAGAATDAEATEADGADGR	5	0

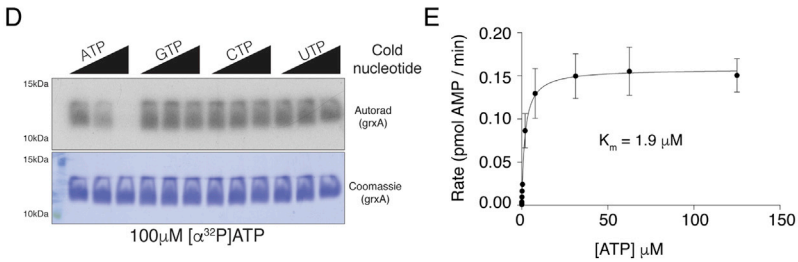

Figure S3. SelO Pseudokinases AMPylate Protein Substrates, Related to Figure 3

(A and B) α-Thr AMP protein immunoblotting of *E. coli* SelO or the inactive D256A mutant (A) or human SelO (U667C) or the inactive D348A mutant (B). The SelO proteins were preincubated with or without Mg^{2+}/ATP prior to SDS-PAGE and immunoblotting. The Ponceau stained membrane is shown as a loading control.

(C) MS/MS data was searched using the Mascot search engine (Matrix Science) for peptide identification and determination of MS2 spectral counts of AMPylated peptide ions. The modification sites were localized to the residues shown in red. When the site could not be assigned to a single residue, all possible sites are shown in red. SelO proteins were digested with trypsin prior to LC-MS/MS.

(D) SelO prefers ATP over other nucleotides as a cosubstrate. Autoradiograph depicting the incorporation of α-^{32}P AMP from 100 μM [α-^{32}P]ATP into *E. coli* glutaredoxin A (grxA) (See Figure 6) by *E. coli* SelO in the presence of 0, 0.1mM or 2mM unlabeled "cold" ATP, GTP, CTP or UTP. The reaction products were resolved by SDS-PAGE and visualized by Coomassie blue staining (lower) and autoradiography (upper).

(E) Kinetic analysis depicting the concentration dependence of Mg^{2+}/ATP on the rate of AMP incorporation into grxA (see Figure 6) by *E. coli* SelO. (*Inset*) K_m for Mg^{2+}/ATP is indicated. Reaction products were analyzed as in Figure 4B.

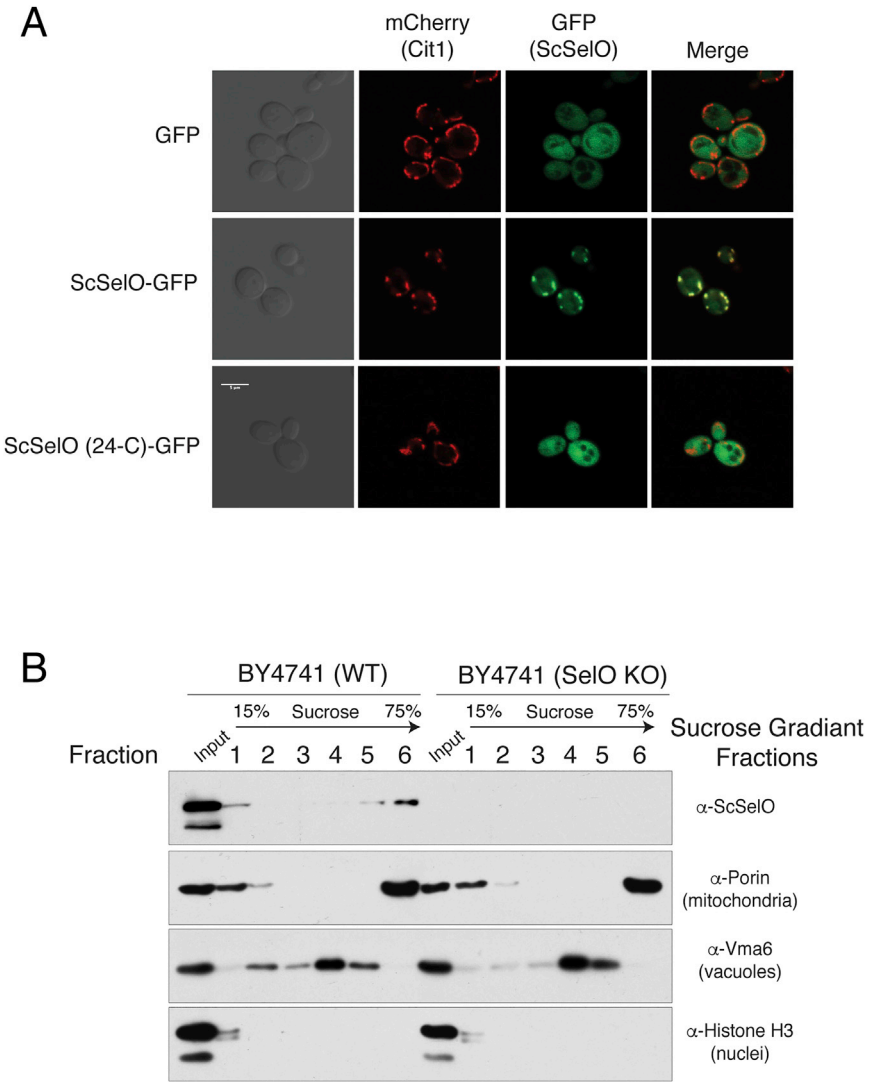

Figure S4. *S. cerevisiae* SelO Localizes to the Mitochondria in Yeast, Related to Figure 5

(A) Confocal images depicting GFP, cit1 mCherry, SelO-GFP or SelO (24-C)-GFP. mCherry was knocked-in to the endogenous locus of *CIT1* to create a C-terminal fusion protein and GFP, SelO-GFP or SelO (24-C)-GFP were expressed in cit1 mCherry cells under the control of a galactose inducible promoter (pDGFP). Phase contrast images are also shown.

(B) Protein immunoblotting of yeast extracts fractionated by sucrose gradient centrifugation. *S. cerevisiae* SelO (ScSelO), porin (mitochondria), Vma6 (vacuoles) and Histone H3 (nuclei) immunoblots are shown.

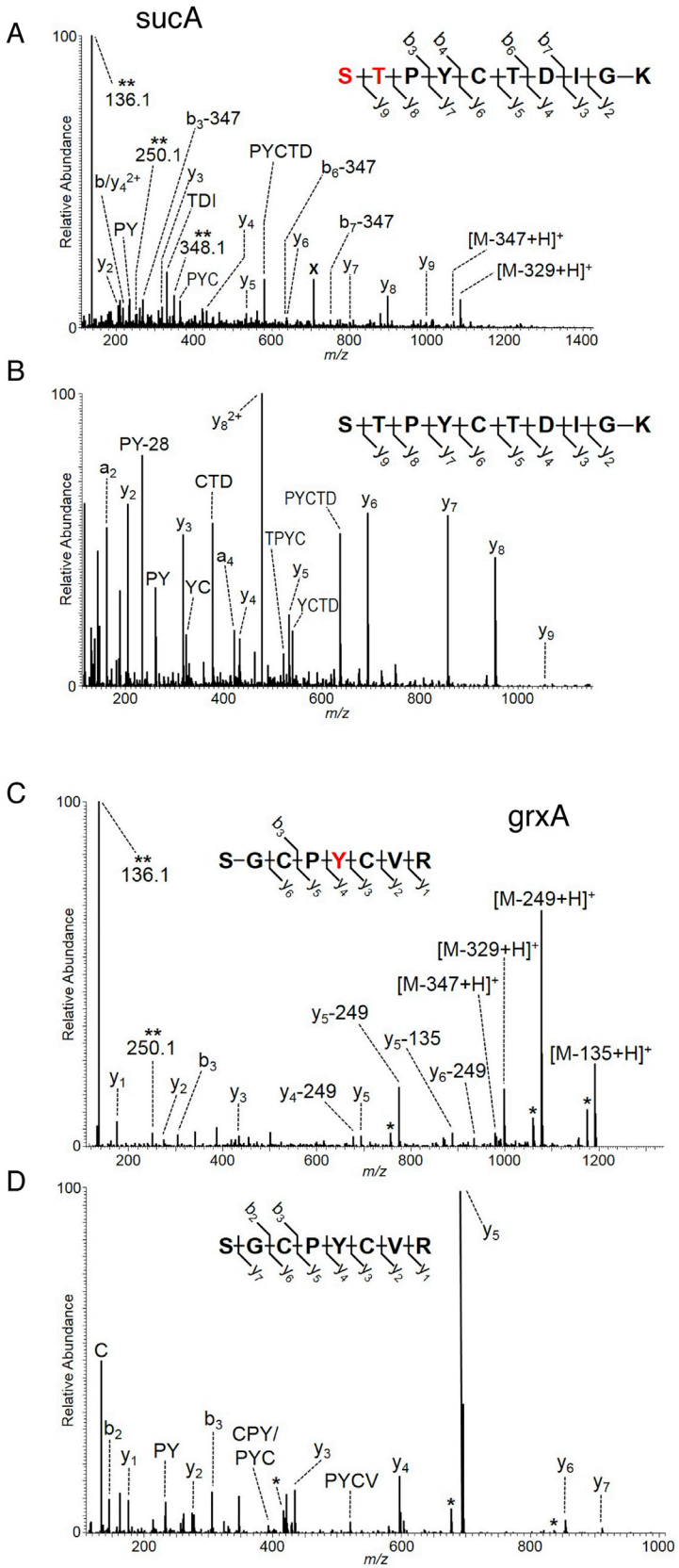

(legend on next page)

Figure S5. *E. coli* SelO AMPylates sucA and grxA in Cells, Related to Figure 6

(A and B) MS/MS spectra of sucA peptide ion STPYCTDIGK. AMPylation was detected on sucA that was coexpressed with *E. coli* SelO (A), while only the unmodified peptide was detected on sucA when coexpressed with the catalytically inactive D256A mutant of *E. coli* SelO (B). Location of the AMP group on the peptide in (A) can be localized to either the serine or threonine reside highlighted in red. The precursor ions, (A) *m/z* 707.28 (2+) (labeled with "X") and (B) *m/z* 571.26 (2+), were subjected to HCD fragmentation to generate the MS/MS spectra shown. B-type fragment ions containing the modified reside in (A) show characteristic mass shifts corresponding to loss of the AMP group (−347 Da). Unique ions corresponding to neutral loss of the AMP group (labeled with **) are also present in (A) at 136.1, 250.1, and 348.1 Da.

(C and D) MS/MS spectra of grxA peptide ions (C) SGCPY(amp)CVR and (D) SGCPYCVR. AMPylation of tyrosine-27 was detected on grxA when coexpressed with *E. coli* SelO (C), while only the unmodified peptide was detected on grxA when coexpressed with the catalytically inactive D256A mutant of *E. coli* SelO DA protein (D). The precursor ions, (C) *m/z* 664.24 (2+) and (D) *m/z* 499.71 (2+), were subjected to HCD fragmentation to generate the MS/MS spectra shown. Fragment ions containing the modified tyrosine residue in (C) show characteristic mass shifts corresponding to loss of the AMP group (−135, −249, −329, and −347 Da). Unique ions corresponding to neutral loss of the AMP group (labeled with **) are also present in (C) at 136.1 and 250.1 Da. Peaks labeled with a single asterisk (*) in both spectra correspond to neutral loss of ammonia (−17 Da) or water (−18 Da) from fragment ions.

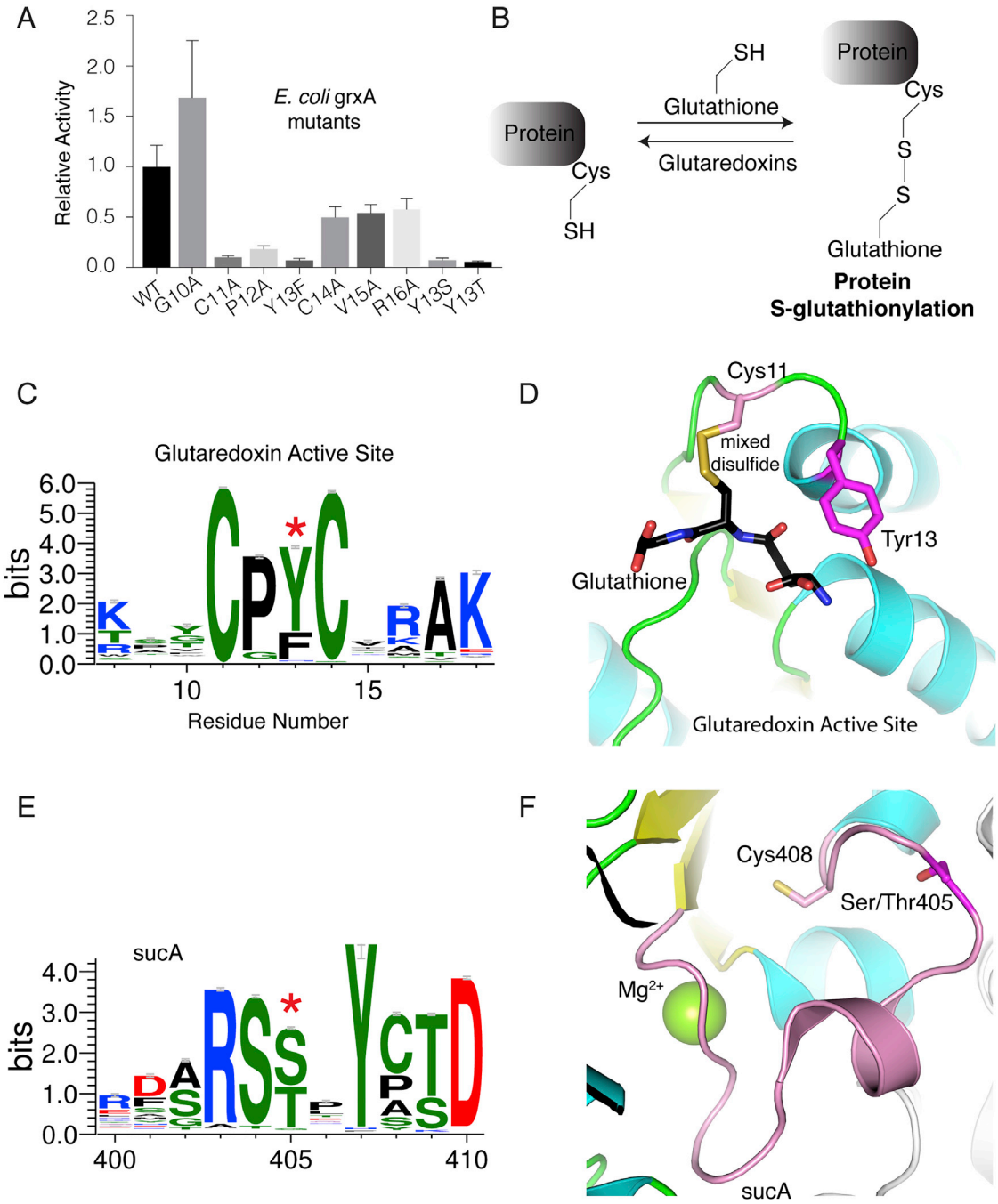

Figure S6. grxA and sucA Are AMPylated on Highly Conserved Active Site Residues, Related to Figure 7

(A) AMPylation activity of *E. coli* SelO using grxA (or mutants) and [α-^{32}P]ATP as substrates. Reaction products were resolved by SDS-PAGE and radioactive gel bands were excised and quantified by scintillation counting.

(B) Protein Cys residues can be modified by a molecule of glutathione (termed Protein S-glutathionylation) to protect them from irreversible over oxidation during oxidative stress conditions. Members of the glutaredoxin family of enzymes remove the glutathione and regenerate the free thiol.

(C) Sequence logo highlighting the conserved active site residues in the grx family of enzymes. The height of the amino acid stack indicates the sequence conservation at that position. The AMPylated Tyr is highlighted with a red asterisk. Logo created using 4105 aligned grxA homologs collected by a Jackhmmer search in the Reference Proteomes database.

(D) Zoomed in view of *E. coli* grxA in cartoon colored by secondary structure: helix (cyan), strand (yellow), and loop (green). GrxA Tyr13 (magenta) is adjacent to the Cys11 (pink stick) that forms a mixed disulfide with glutathione (black stick). PDB: 1grx

(legend continued on next page)

(E) Sequence logo highlighting the conserved residues surrounding the AMPylation site in sucA (E1 component of the alpha ketoglutarate dehydrogenase) family of enzymes. The height of the amino acid stack indicates the sequence conservation at that position. The AMPylated Thr is highlighted with a red asterisk. Logo created using 7591 aligned sucA homologs collected by a Jackhmmer search.

(F) Zoomed in view of *E. coli* sucA in cartoon colored by secondary structure: helix (cyan), strand (yellow), and loop (green). SucA Thr405 (magenta) is adjacent to Cys408 (pink stick) in a loop (pink) that coordinates Mg^{2+} (green sphere) and mediates dimerization (interacting chain in white cartoon) in a closely related *Mycobacterium smegmatis* structure (Note that the *E.coli* sucA loop containing Thr405 is disordered). PDB: 2xta

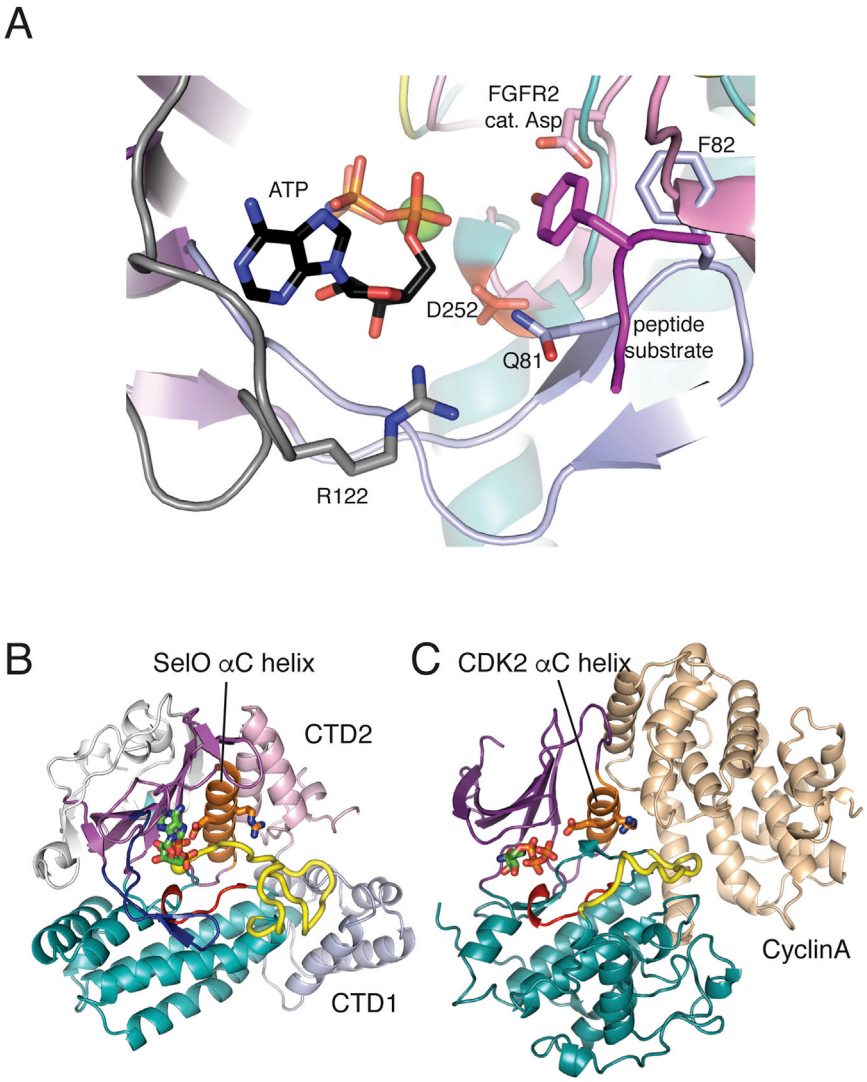

Figure S7. The SelO Structure Reveals Insights into Substrate Recognition and Regulation, Related to Figure 4

(A) Potential SelO peptide binding site. Closeup view of the SelO kinase domain (colored as previously) superimposed with activated FGFR2 kinase domain (PDB:2pvf: activation and catalytic loop displayed in pink cartoon, with catalytic Asp in stick) bound to substrate peptide (magenta, with Tyrosine in stick) reveals the approximate position of a docked SelO peptide substrate. Conserved SelO residues near the peptide binding site are in stick, including the migrated active site Asp (D252, red stick) and others (Q81, F82, and R122).

(B and C) SelO C-terminal domains mimic Cyclin A activation of CDK2. (B) SelO kinase N-lobe (purple) αC helix (orange) is positioned by CTD2 (pink) with a conserved αC-helix RE motif (stick) interacting with the substrate analog (stick) and with the activation loop (yellow) from the C-lobe (teal). (C) Cyclin A (wheat) positions a similar conserved motif in CDK2 (depicted as above).